Cell

The life-saving benefit of dexamethasone in severe COVID-19 is linked to a reversal of monocyte dysregulation

Graphical abstract

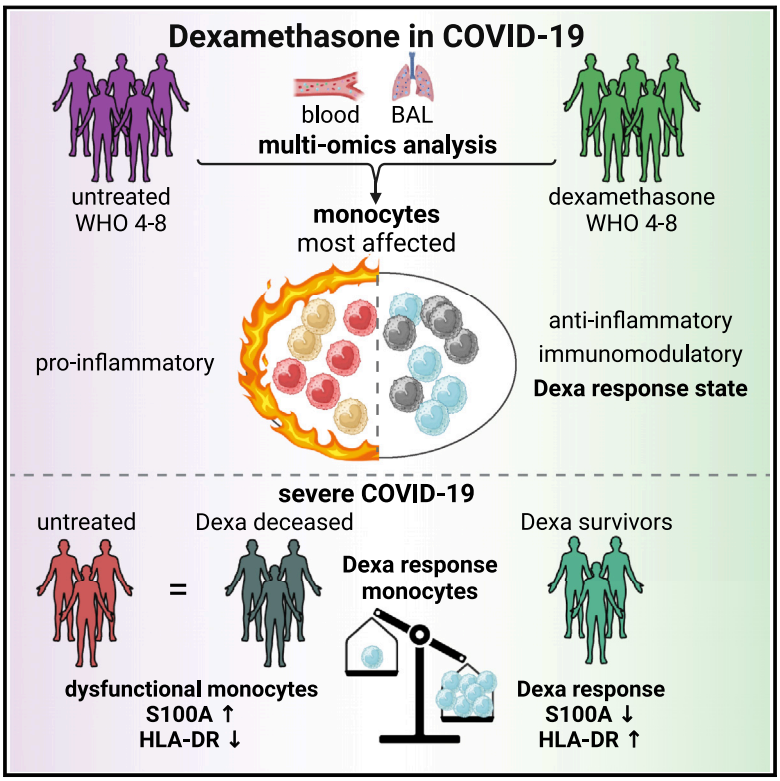

Highlights

- Dexamethasone-induced transcriptional changes were confined to a specific monocyte state
- Molecular treatment responses in monocytes were directly linked to clinical outcome
- Reversal of dysregulated monocyte signatures in dexamethasone-treated COVID-19 survivors
- Monocyte single-cell signatures stratified blood samples for treatment response

Authors

Rainer Knoll, Elisa T. Helbig, Kilian Dahm, ..., Joachim L. Schultze, Anna C. Aschenbrenner, Florian Kurth

Correspondence

anna.aschenbrenner@dzne.de

In brief

Dexamethasone was used as an effective drug for severe COVID cases during the pandemic. A study integrating single-cell and bulk transcriptomics in clinical cohorts reveals the molecular basis of its immunomodulatory effect and also provides a framework for the future development of companion diagnostics for patient stratification in precision medicine.

Knoll et al., 2024, Cell *187*, 4318–4335
August 8, 2024 © 2024 The Authors. Published by Elsevier Inc.
https://doi.org/10.1016/j.cell.2024.06.014

CellPress

CellPress
OPEN ACCESS

Cell

Article

The life-saving benefit of dexamethasone in severe COVID-19 is linked to a reversal of monocyte dysregulation

Rainer Knoll,[1,20] Elisa T. Helbig,[2,20] Kilian Dahm,[1,3] Olufemi Bolaji,[4] Frederik Hamm,[5] Oliver Dietrich,[6] Martina van Uelft,[1,7] Sophie Müller,[1,7,8] Lorenzo Bonaguro,[1,9] Jonas Schulte-Schrepping,[1,9] Lev Petrov,[4] Benjamin Krämer,[10] Michael Kraut,[9] Paula Stubbemann,[2] Charlotte Thibeault,[2,11] Sophia Brumhard,[2] Heidi Theis,[9] Gudrun Hack,[10] Elena De Domenico,[9] Jacob Nattermann,[10] Matthias Becker,[1] Marc D. Beyer,[1,9,12] David Hillus,[2] Philipp Georg,[2] Constantin Loers,[2] Janina Tiedemann,[2] Pinkus Tober-Lau,[2] Lena Lippert,[2] Belén Millet Pascual-Leone,[2] Frank Tacke,[13] Gernot Rohde,[14,15,16] Norbert Suttorp,[2,16,17] Martin Witzenrath,[2,16,17] CAPNETZ Study Group, Pa-COVID-19 Study Group, Antoine-Emmanuel Saliba,[6,18] Thomas Ulas,[1,7,9] Julia K. Polansky,[5,19] Birgit Sawitzki,[4] Leif E. Sander,[2,5,17,20] Joachim L. Schultze,[1,7,9,20] Anna C. Aschenbrenner,[1,20,21,*] and Florian Kurth[2,17,20]

[1]Systems Medicine, Deutsches Zentrum für Neurodegenerative Erkrankungen (DZNE), Bonn, Germany
[2]Department of Infectious Diseases and Critical Care Medicine, Charité - Universitätsmedizin Berlin, Berlin, Germany
[3]Translational Pediatrics, Department of Pediatrics, University Hospital Würzburg, Würzburg, Germany
[4]Institute of Medical Immunology, Charité - Universitätsmedizin Berlin, Berlin, Germany
[5]BIH Center for Regenerative Therapies (BCRT), Berlin Institute of Health at Charité - Universitätsmedizin Berlin, Berlin, Germany
[6]Helmholtz Institute for RNA-based Infection Research (HIRI), Helmholtz-Center for Infection Research (HZI), Würzburg, Germany
[7]Genomics & Immunoregulation, Life & Medical Sciences Institute, University of Bonn, Bonn, Germany
[8]Department of Microbiology and Immunology, The University of Melbourne at the Peter Doherty Institute for Infection and Immunity, Melbourne, VIC, Australia
[9]PRECISE Platform for Single Cell Genomics and Epigenomics, DZNE, University of Bonn, and West German Genome Center, Bonn, Germany
[10]Department of Internal Medicine I, University Hospital Bonn, Bonn, Germany
[11]BIH Biomedical Innovation Academy, BIH Charité Clinician Scientist Program, Berlin Institute of Health at Charité - Universitätsmedizin Berlin, Berlin, Germany
[12]Immunogenomics & Neurodegeneration, Systems Medicine, Deutsches Zentrum für Neurodegenerative Erkrankungen (DZNE), Bonn, Germany
[13]Department of Hepatology and Gastroenterology, Charité - Universitätsmedizin Berlin, Berlin, Germany
[14]Department of Respiratory Medicine, Medical Clinic I, Goethe-Universität Frankfurt am Main, Frankfurt, Germany
[15]Biomedical Research in Endstage and Obstructive Lung Disease Hannover (BREATH), Member of the German Center for Lung Research (DZL), Hannover, Germany
[16]CAPNETZ STIFTUNG, 30625 Hannover, Germany
[17]German Center for Lung Research (DZL), Germany
[18]Faculty of Medicine, Institute of Molecular Infection Biology (IMIB), University of Würzburg, Josef-Schneider-Str. 2, 97080 Würzburg, Germany
[19]German Rheumatism Research Centre (DRFZ) Berlin, Berlin, Germany
[20]These authors contributed equally
[21]Lead contact
*Correspondence: anna.aschenbrenner@dzne.de
https://doi.org/10.1016/j.cell.2024.06.014

SUMMARY

Dexamethasone is a life-saving treatment for severe COVID-19, yet its mechanism of action is unknown, and many patients deteriorate or die despite timely treatment initiation. Here, we identify dexamethasone treatment-induced cellular and molecular changes associated with improved survival in COVID-19 patients. We observed a reversal of transcriptional hallmark signatures in monocytes associated with severe COVID-19 and the induction of a monocyte substate characterized by the expression of glucocorticoid-response genes. These molecular responses to dexamethasone were detected in circulating and pulmonary monocytes, and they were directly linked to survival. Monocyte single-cell RNA sequencing (scRNA-seq)-derived signatures were enriched in whole blood transcriptomes of patients with fatal outcome in two independent cohorts, highlighting the potential for identifying non-responders refractory to dexamethasone. Our findings link the effects of dexamethasone to specific immunomodulation and reversal of monocyte dysregulation, and they highlight the potential of single-cell omics for monitoring *in vivo* target engagement of immunomodulatory drugs and for patient stratification for precision medicine approaches.

 © 2024 The Authors. Published by Elsevier Inc.
This is an open access article under the CC BY-NC-ND license (http://creativecommons.org/licenses/by-nc-nd/4.0/).

INTRODUCTION

Dexamethasone represents the first and most effective treatment against severe COVID-19,[1] with likely millions of lives saved worldwide during the COVID-19 pandemic. Based on transcriptome-based reverse drug target prediction, we had identified dexamethasone as a potential drug candidate for a subgroup of patients with severe disease courses.[2] As early as June 2020, preliminary data from the Randomized Evaluation of COVID-19 Therapy (RECOVERY) platform trial demonstrated a significant clinical benefit of dexamethasone, reducing the relative risk of 28-day mortality by approximately 30% in patients with severe COVID-19 requiring mechanical ventilation.[1] The benefit of glucocorticoid (GC) treatment in severe COVID-19 was subsequently validated in further trials[1,3,4] and dexamethasone quickly became the standard of care (SOC) for all patients with COVID-19 requiring supplemental oxygen or mechanical ventilation.[5] The survival benefit was lower in patients requiring supplemental oxygen therapy without invasive ventilation, whereas no benefit and even harm was observed in patients without respiratory failure and no need for supplemental oxygen, particularly at higher doses.[1,6,7] Although no impact of dexamethasone on severe acute respiratory syndrome coronavirus 2 (SARS-CoV-2) viral load kinetics, antibody and T cell response was observed with the standard dexamethasone dose used in the RECOVERY trial,[8,9] negative effects of corticosteroid use have previously been reported for patients with viral pneumonia caused by SARS-CoV and Middle East respiratory syndrome-related coronavirus (MERS-CoV),[10] where delayed viral clearance was observed, as well as for influenza, where corticosteroid therapy is associated with higher mortality.[11]

As no mechanistic studies were conducted in the pivotal clinical efficacy trials, smaller experimental studies have elaborated on the potential effects of corticosteroids on the immune system. A recent study demonstrated that dexamethasone treatment of patients with severe COVID-19 affected circulating neutrophils. The study revealed transcriptional alteration of several of the known neutrophil cell states in peripheral blood, mainly counteracting sustained interferon (IFN) activation and reinforcing suppressor states, suggesting limitation of neutrophil pathogenicity.[12] In two hamster models, a strong anti-inflammatory effect of dexamethasone was postulated as a major effect of therapy, which was also linked to a specifically responsive subpopulation of neutrophils.[13] Downregulation of STAT1 target genes in monocytes[14] as well as suppression of T cell function[15] were two other potential modes of action of dexamethasone in COVID-19, yet a link of these transcriptomic changes to treatment response and clinical outcome is missing.

Despite the proven clinical effectiveness of dexamethasone, a substantial number of patients progresses to critical illness and die from COVID-19 with apparently little or no response to dexamethasone treatment. Overall, the mechanisms of action of dexamethasone in severe COVID-19 are unknown, and biomarkers of treatment response or treatment failure are missing. Early prediction of treatment failure, however, would be valuable to guide early step-up of immunomodulatory therapy, and results from recent clinical trials assessing efficacy of dexamethasone in COVID-19 further support the need for biomarker-supported clinical decision processes, even for such well-known and widely used drugs as corticosteroids.[6,16]

Here, we provide a framework to identify molecular modes of action and markers of treatment response of repurposed drugs, exemplified by dexamethasone in COVID-19. We identified patients treated with and without dexamethasone according to criteria of the RECOVERY trial during the first months of the COVID-19 pandemic from a large observational cohort study.[17] We generated single-cell omics profiles from peripheral blood-derived immune cells, deciphered cellular, molecular, and functional changes to dexamethasone treatment, and linked the observed changes to clinical outcomes. We found that dexamethasone specifically reverses the dysfunctional molecular phenotypes associated with severe COVID-19 in monocytes of patients with a clinical response to treatment but not those with a fatal outcome. Based on these outcome-specific single-cell gene expression data, we generated transcriptomic signatures that we transferred to whole blood transcriptomes of two independent COVID-19 cohorts, demonstrating their potential as predictive biomarkers for treatment response in clinical studies. We reveal molecular hallmarks that are linked to the life-saving effects of dexamethasone and demonstrate, in general, the feasibility of single-cell transcriptomics to assess *in vivo* drug target engagement and treatment responses in clinical studies.

RESULTS

Dexamethasone treatment leads to immunomodulation in circulating immune cells

To determine cellular and molecular changes induced by dexamethasone treatment in COVID-19 patients, we identified all patients enrolled in our central phenotyping platform study[17] who were infected during the first two waves of the COVID-19 pandemic (i.e., infected with SARS-CoV-2 D614G strain) and who were either GC naive (first wave from March to May 2020, termed control patients, short "ctrl") or who were treated with dexamethasone (second wave from October 2020 to February 2021) (Figure 1A; Table S1).[17] We carefully selected patients who met the criteria for dexamethasone treatment as identified in the RECOVERY trial. Of note, all selected patients did not receive any other immunomodulatory or any antiviral treatment. We selected patients who received dexamethasone or were treatment-naive and matched them for sex, age, disease severity, and time from symptom onset to blood sampling, resulting in comparable baseline characteristics and disease severity (Table S1). Whole blood and peripheral blood mononuclear cells (PBMCs) were taken on average 8 days after treatment initiation and subjected to high-dimensional single-cell analyses utilizing cytometry by time of flight (CyTOF), single-cell RNA sequencing (scRNA-seq), and multi-color flow cytometry.

Assessment of compositional alterations of the major immune cell types (Figure 1B) by CyTOF revealed significantly increased leukocytes in dexamethasone-treated patients with moderate disease severity (Figure 1C). Increased leukocyte frequencies were mainly due to alterations in B cells and neutrophils in moderately ill patients (hospitalized patients requiring oxygen supplementation but no mechanical ventilation), while there

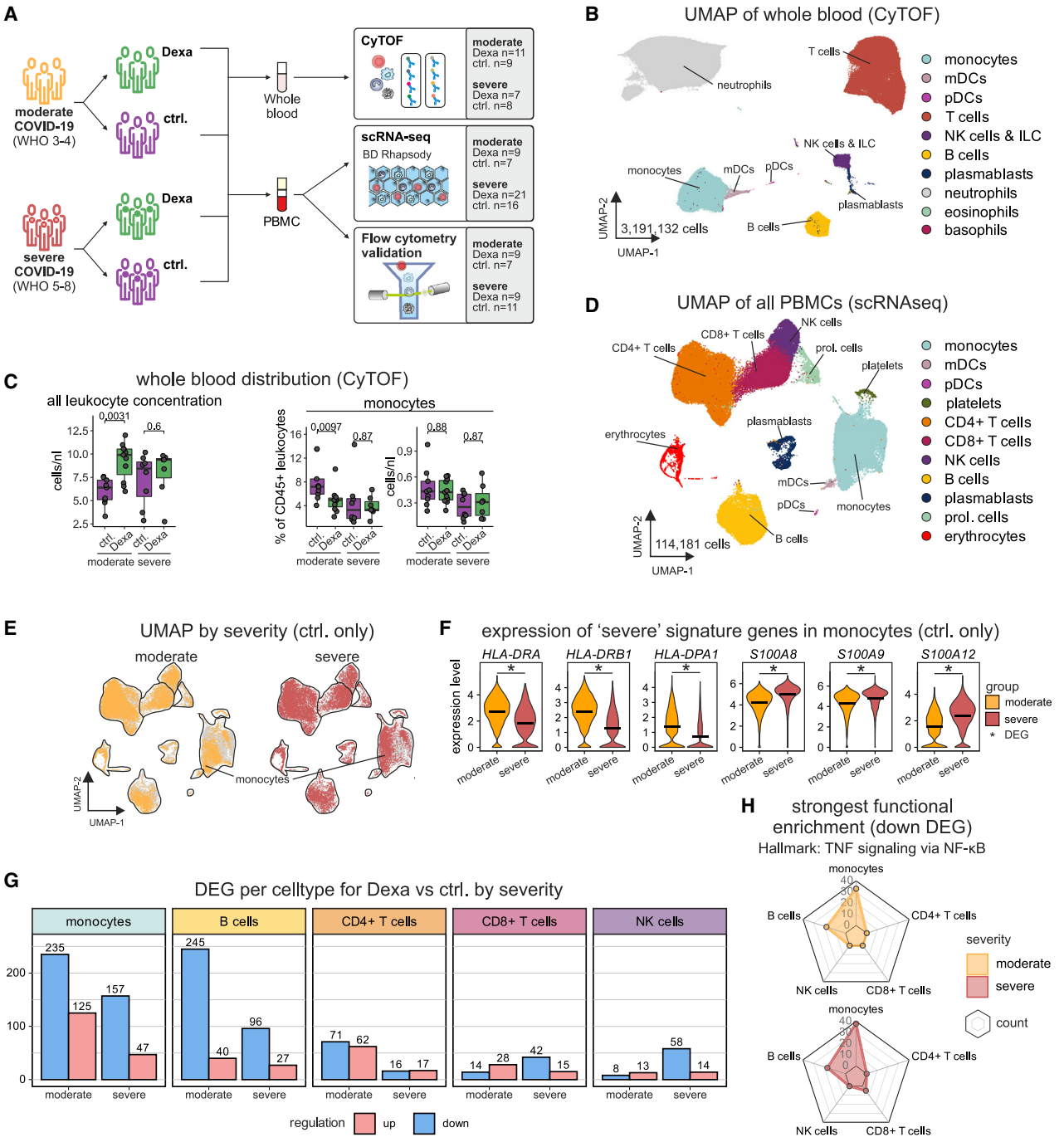

Figure 1. Dexamethasone treatment leads to immunomodulation in circulating immune cells

(A) Study design: hospitalized moderately (supplemental oxygen needed) and severely affected (i.e., intensive care unit treatment) patients with COVID-19 treated with dexamethasone were matched for sex, age, disease severity, and time from symptom onset to blood sampling with treatment-naive COVID-19 patients (ctrl.). Samples were obtained prior to treatment or corresponding time points for controls ("early"), respectively, and toward the end of the treatment period and corresponding time points for controls ("late"). Whole blood leukocytes were analyzed by CyTOF, and purified PBMCs were analyzed by scRNA-seq and flow cytometry for marker validation. Included sample numbers are indicated. See Table S1.

(B) UMAP of whole blood cells (downsampled from n = 3,191,132 to n = 986,030 cells for better visualization) from CyTOF with identified cell types indicated.

(C) Absolute leukocyte counts from differential blood count, monocyte percentages, and concentration of whole blood cells from CyTOF. Wilcoxon test for statistical significance, and resulting p value is indicated.

(D) UMAP visualization of the entire PBMC space (n = 114,181 cells) from scRNA-seq with indicated major cell types.

(legend continued on next page)

was no difference in dexamethasone-treated severely ill patients (Figure S1A). Further, there was a relative decrease of monocytes in dexamethasone-treated patients with moderate disease (Figure 1C). Altogether, the compositional changes indicated cell-type-related immunomodulatory alterations of dexamethasone treatment.

Next, we defined molecular phenotypes and treatment-related transcriptional alterations of a total of 114,181 PBMCs by scRNA-seq. All major blood-derived immune cell types were present in our dataset (Figures 1D and S1B). Overlaying time of sampling after symptom onset ($\leq$10 and >10 days, Figure S1C) or disease severity onto the uniform manifold approximation and projection (UMAP) (Figure 1E) revealed global distribution shifts, as previously described,[18] particularly within the monocyte compartment. Specifically, we observed profound disease severity-related alterations in expression of human leukocyte antigen (HLA) and S100A genes (Figure 1F) and the IFN system (Figure S1D), as previously described.[18] In order to reveal transcriptional effects of dexamethasone treatment, we quantified differentially expressed genes (DEGs) by cell type (Figure 1G). We observed the strongest treatment-dependent transcriptional changes in monocytes, followed by B cells and $CD4^+$ T cells, with all other cell types showing a moderate gene regulation. Of note, we observed an upregulation of a substantial number of genes associated with dexamethasone treatment in monocytes in moderate and severe disease (Figure 1G). Despite clear differences in the magnitude of transcriptional alterations between cell types, we identified a small set of DEGs shared across cell types in severe COVID-19, including the well-known GC receptor target genes *TSC22D3*[19] and *TXNIP*[20] among the commonly upregulated genes, while *IFITM1* and *FTH1* were among the downregulated genes (Figure S1E). Functional enrichment analysis across all major cell types using all up- and downregulated genes revealed that a large number of genes are tumor necrosis factor alpha (TNF)-mediated nuclear factor κB (NF-κB) target genes, particularly within downregulated DEGs (Figures 1H and S1F), which corroborates previous findings that corticosteroids can inhibit NF-κB transcription factor family members.[21,22] The importance of dexamethasone-related changes in the monocyte compartment was further illustrated by the strongest enrichment scores of many other cellular functions when assessing upregulated DEGs in patients with severe disease (Figure S1F, right panel).

In summary, we observed transcriptional changes associated with dexamethasone treatment that were quantitatively most prominent in monocytes and B cells and exhibited cell-type-specific modulations in addition to common transcriptional changes.

Dexamethasone treatment elicits a unique cell state in a subset of monocytes

To determine disease severity-dependent commonalities and differences in the transcriptional response of monocytes to treatment, we compared DEGs in monocytes from dexamethasone-treated (Dexa) vs. untreated (ctrl.) patients with severe and moderate COVID-19 (Figure 2A). Dexamethasone treatment suppressed expression of several proinflammatory genes, including *IL1B*, *CCL3*, *CCL4*, *CCL3L3*, and *CCL4L2*, irrespective of disease severity, and induced a disease severity-independent gene program, which included known GC-response genes such as *IL1R2*, the decoy receptor for interleukin (IL)-1 in line with the anti-inflammatory effect of dexamethasone, as well as *TSC22D3, CD163*, *SAP30*, *PER1*, and *ZFP36L2*[19,23–25] (Figure 2B). Based on these *in vivo* changes, we compiled a dexamethasone treatment gene signature composed of both down- and upregulated genes (Figure 2C). Upregulated genes were functionally related to hypoxia and regulation of catabolic processes, while downregulated genes enriched for NF-κB signaling and terms related to immune activation (Figure 2D). Further, we found a GC signature derived from monocytes treated with a synthetic GC *in vitro*[26] to be strongly enriched in monocytes during dexamethasone treatment in our dataset (Figure 2E).

Next, we sub-clustered the 23,416 transcriptomes of the monocyte space into ten different cell states (Figures 2F and 2G), showing enrichment of seven cell state signatures derived from acute COVID-19 prior to introduction of dexamethasone therapy[18] (Figure S2A). Despite the enrichment of the GC-response gene signature upon dexamethasone treatment in the monocyte space overall (Figure 2E), cell state-specific analysis revealed the strongest enrichment of the GC signature in one selected cluster, which we termed "Dexa response" cell state (Figures 2H and S2B). These findings were validated with gene sets based on the Gene Ontology (GO) term "response to GC" and "response to steroid hormone" (Figures 2I and 2J). Manual assessment of individual genes corroborated the Dexa response state to be related to dexamethasone treatment as several known GC target genes were elevated including *TSC22D3*,[19] *SAP30*,[24] *FKBP5*,[27] and *CD163*[23] (Figure 2G). To cross-validate our results, we analyzed 2,350 monocyte transcriptomes included in a recently published dataset of dexamethasone-treated patients,[12] revealing similar changes in monocytes from this independent dataset (Figures S2C and S2D).

Dexamethasone treatment elicited a transcriptional core signature in monocytes in COVID-19 patients, independent of disease severity. Single-cell analysis revealed that these

(E) UMAP of the entire PBMC space by scRNA-seq colored by COVID-19 severity with indicated cell types subsetted for untreated controls. Shift in monocytes is indicated.

(F) Violin plots indicating the expression of selected MHC class II (*HLA-DRA*, *HLA-DRB1*, and *HLA-DPA1*) and alarmin (*S100A8*, *S100A9*, and *S100A12*) genes by severity in monocytes of untreated controls. Significant differential expression is indicated with asterisks.

(G) Number of differentially expressed (DE) genes (DEGs) by major cell type with at least 2,000 cells for dexamethasone vs. control by COVID-19 severity (DE parameters: $\log_2$FC = 0.25, min.pct = 0.1).

(H) Spider plots depicting the Hallmark TNF signaling via NF-κB, the most prominent term of functional enrichment analysis for the dexamethasone downregulated genes by cell types extracted from Figure S1F.

See also Figure S1.

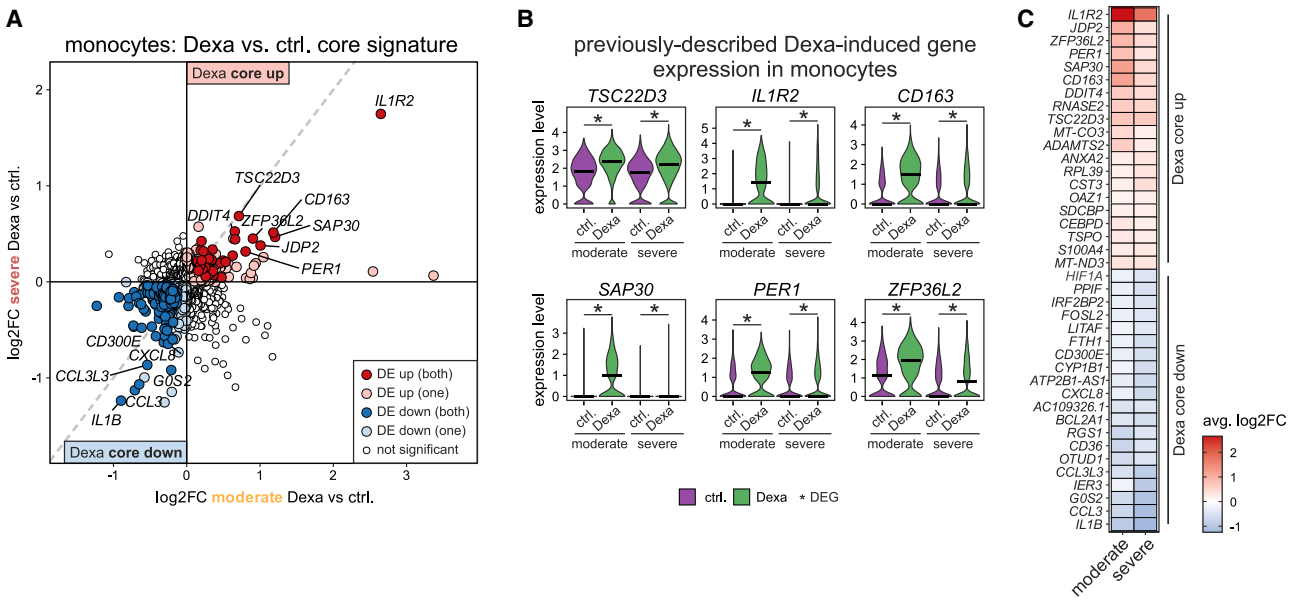

(legend on next page)

transcriptional changes were not present evenly across all monocytes, but that a specific monocyte substate elicited upon dexamethasone treatment showed the highest enrichment of GC-response genes (Dexa response monocyte state).

Dexamethasone-induced transcriptional modulation of monocytes is linked to clinical outcome

Although clinical trials have demonstrated a strong clinical benefit of dexamethasone in patients with moderate and severe COVID-19, a substantial number of patients—almost 30% in the RECOVERY trial—died despite dexamethasone treatment.[1] It is unclear whether the unfavorable outcome in these patients is caused by a failure to adequately respond to treatment and which mechanisms contribute to a treatment benefit. We therefore assessed whether the distribution of treatment-related monocyte cell states was linked to disease severity and to the clinical outcome. The Dexa response monocyte state was prevalent in up to 80% of all monocytes in dexamethasone-treated patients with moderate COVID-19 (hospitalized patients requiring oxygen supplementation but no mechanical ventilation) and less pronounced in dexamethasone-treated patients with severe COVID-19 (Figure 3A). Similarly, protein expression of CD163, a prominent marker gene of the dexamethasone response cluster, was elevated on monocytes in dexamethasone-treated COVID-19 patients (Figure S3A). Analysis of whole blood samples by CyTOF (Figure S3B) revealed that cluster abundance of the $CD14^{+}CD16^{-}CD163^{hi}$ classical monocytes (Figure 3B) and signal intensity of CD163 (Figure 3C) were significantly elevated in dexamethasone-treated patients, whereas the $CD14^{+}$ and $CD16^{+}$ $CD69^{+}PD\text{-}L1^{+}$ activated classical and non-classical monocyte subpopulations were significantly downregulated by dexamethasone treatment (Figure S3C), with potentially beneficial effects on T cell functionality, similar to programmed cell death ligand-1 (PD-L1) blockade in SARS-CoV-2 infection.[28]

Further stratification of dexamethasone-treated patients with severe COVID-19 by clinical outcome (survival) revealed a significantly higher frequency of Dexa response monocytes in survivors compared with patients who later died during the course of their disease (deceased), in whom Dexa response state monocytes were low to undetectable (Figures 3D and S3D).

Given the outcome-dependent transcriptional changes, we next contrasted the DEGs in all monocytes focusing on dexamethasone-treated surviving patients (i.e., responders) and untreated control survivors (Figure 3E). Beyond the downregulation of proinflammatory genes observed in the dexamethasone core signature, selective analysis of monocyte gene expression in survivors revealed that dexamethasone treatment was associated with a reversal of the previously reported transcriptional dysregulation in monocytes in severe COVID-19.[18] Dexamethasone treatment led to a downregulation of alarmins, cytokines, and chemokines and reconstitution of *HLA-DRB1*, *HLA-DRA*, *HLA-DPA1*, and *CD74* expression (Figure 3F). Alarmin expression in monocytes was lower at 7 days compared with 3 days after initiation of dexamethasone treatment[12] (Figure S3E), indicating a time-dependent effect of dexamethasone on alarmin gene expression.

In line with these findings, dexamethasone treatment significantly reduced the frequency of $S100A^{hi}$ monocytes in survivors, but not in non-survivors (Figure 3G). Differential gene expression analysis of patients with severe COVID-19 (all treated with dexamethasone) showed that dexamethasone induced the upregulation of genes associated with a milder course of disease, specifically in survivors, whereas monocytes in non-survivors expressed higher levels of alarmins associated with monocyte dysregulation (Figure 3H), resembling untreated patients with severe COVID-19 (Figure S3F). These data indicated that a non-favorable clinical outcome, i.e., death from COVID-19, was associated with a failure of monocytes to respond to dexamethasone. We had previously identified a dysregulated monocyte state marked by low major histocompatibility complex (MHC)-II expression and high levels of alarmins, termed "$HLA\text{-}DR^{lo}S100A^{hi}$," which was strongly associated with COVID-19 severity.[18] Gene set enrichment analysis (GSEA) showed that dexamethasone treatment reversed this dysfunctional monocyte phenotype in survivors, whereas monocytes from deceased patients did not show a reversal of this transcriptional signature, hence failed to respond to treatment (Figure 3I).

In addition to monocytes, we also tested B cells for outcome-specific signatures, as they also showed profound transcriptional changes to dexamethasone (Figure 1G). However, only a

Figure 2. Dexamethasone elicits a unique cell state in a fraction of monocytes

(A) Fold change-fold change (FC-FC) plot showing the $\log_2$ fold changes of differentially expressed genes (DEGs) in monocytes from the comparisons of severe COVID-19 Dexa vs. control (y axis) and moderate COVID-19 Dexa vs. control (x axis). Genes that are DE in both or only one comparison are indicated.

(B) Violin plots depicting expression of previously described dexamethasone-induced genes (*TSC22D3*, *IL1R2*, *CD163*, *SAP30*, *PER1*, and *ZFP36L2*) in monocytes stratified by severity and treatment. Significant differential expression is indicated with asterisks.

(C) Heatmap of the average $\log_2$ fold change in monocytes from genes identified in (A) stratified by the severity comparisons. For representation, the top 20 upregulated and downregulated genes were selected.

(D) Functional enrichment of the Dexa core signature genes from (A) and (C) using the GO and Hallmark databases (Bonferroni-adjusted p value < 0.05).

(E) Enrichment of the *in vitro* generated glucocorticoid signatures from Wang et al.[26] in monocytes stratified by COVID-19 severity and treatment represented as mean module score per donor. Statistical testing using Wilcoxon test.

(F) UMAP visualization of the entire monocyte space (n = 23,416 cells) with identified monocyte states. The Dexa response state is highlighted.

(G) Marker gene expression levels for identified monocyte states from (F). Markers for the Dexa response state are highlighted.

(H) Enrichment of the *in vitro* generated glucocorticoid up signatures from Wang et al.[26] in all monocyte states. Kruskal-Wallis (KW) test between mean module scores by donor and cell states, and the resulting p value is indicated.

(I) Enrichment of the GO term response to glucocorticoid in all monocyte states. Kruskal-Wallis (KW) test between mean module scores by donor and cell states, and the resulting p value is indicated.

(J) Enrichment of the GO term response to steroid hormone in all monocyte states. Kruskal-Wallis (KW) test between mean module scores by donor and cell states, and the resulting p value is indicated.

See also Figure S2.

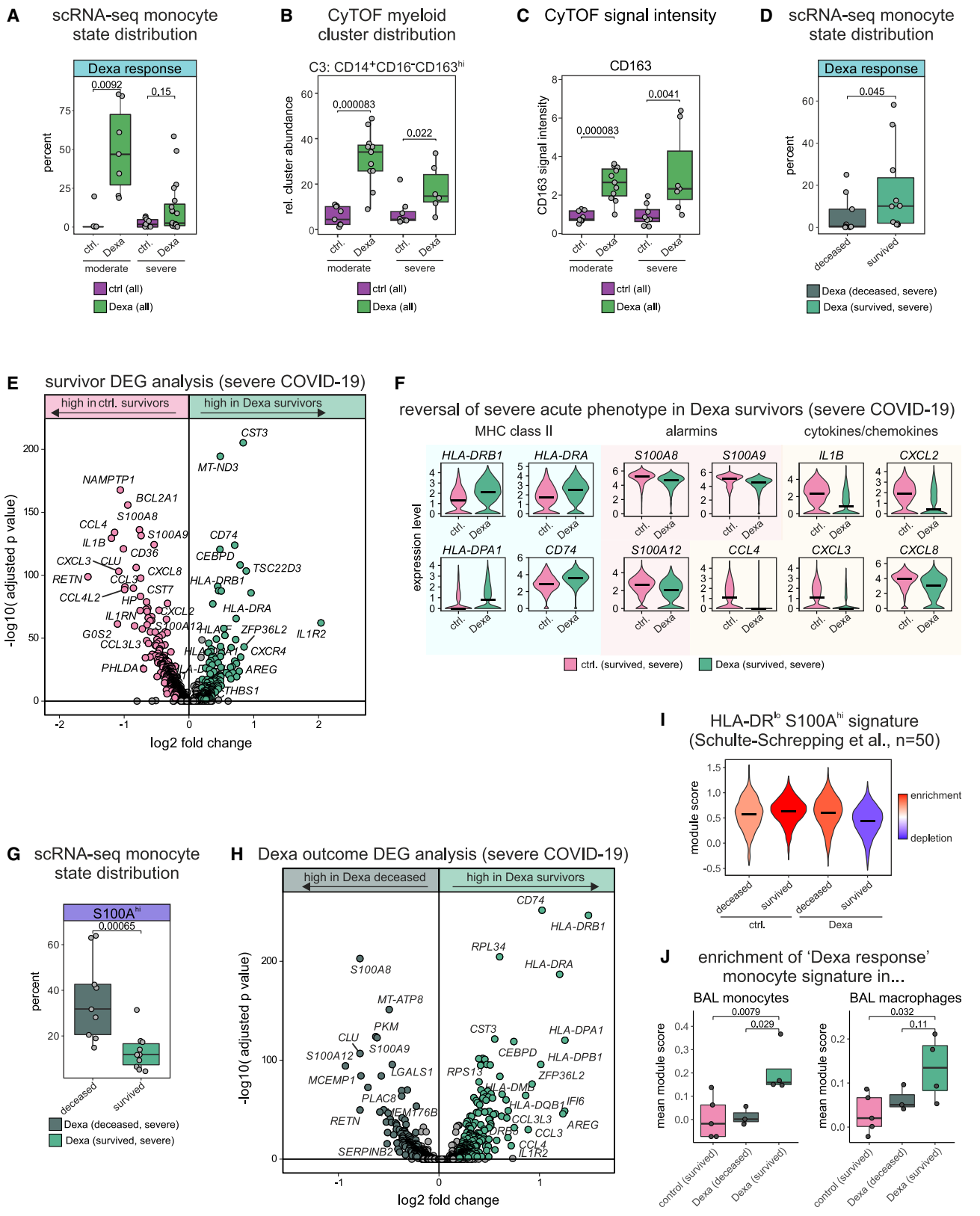

(legend on next page)

comparatively small fraction of genes was associated with outcome, indicating that B cells are not informative in contrast to the monocytes for stratifying treatment response (Figure S3G).

To evaluate if similar treatment effects as detected in blood monocytes were also detectable in the lungs and therefore potentially directly related to organ failure and disease progression, we analyzed cells from bronchoalveolar lavage (BAL) of patients with severe COVID-19. First, we analyzed published single-cell transcriptomes of BAL[29] including a total of six patients with severe COVID-19 patients, four of whom were treated with the synthetic GC methylprednisolone. We recovered similar patterns as we found in blood monocytes in response to dexamethasone treatment. Disease outcome-stratifying markers from the blood monocytes (Figure 3E) were also highly expressed in BAL myeloid cells of methylprednisolone-treated survivors (n = 2), while blood monocyte markers associated with treatment failure were higher in treated deceased patients (n = 2, Figure S3H). As the cohort size in this published dataset was too limited for robust statistical analysis, we generated single-cell transcriptomes from BAL samples collected from twelve patients with severe COVID-19 in the first two waves in Germany, including seven dexamethasone-treated and five untreated patients. The dataset comprised a total of 67,439 cells (Figure S3I; Table S1) and recovered all major cell types expected in BAL (Figures S3J and S3K). In order to investigate similarities of the transcriptional responses to dexamethasone between circulating and pulmonary immune cells, we analyzed the enrichment of the signature of Dexa response monocytes from blood in BAL monocytes and macrophages, stratified by treatment (dexa vs. untreated) and outcome (survival vs. deceased) (Figure 3J). The Dexa response signature was significantly enriched in BAL monocytes from dexamethasone-treated survivors, but it was neither enriched in monocytes from untreated patients nor in dexamethasone-treated deceased patients. A similar stratification was observed in BAL macrophages, albeit to a lesser extent (Figure 3J). These data indicate that transcriptional responses to dexamethasone treatment detected in circulating monocytes are preserved in the lung and likely contribute to outcome benefits of dexamethasone.

In conclusion, induction of a Dexa response monocyte state in patients with severe COVID-19 treated with dexamethasone was associated with clinical benefit (survival). In addition, dexamethasone treatment exerted specific modulatory effects by reversing the dysregulated monocyte phenotype in patients with severe COVID-19, whereas fatal outcome was associated with a failure to revert the dysregulated monocyte phenotype. These data link the clinical effect of a pharmacological intervention (dexamethasone) to a molecular phenotype in immune cells in the blood and in the lung. The data also demonstrate the versatility of scRNA-seq to reveal mechanisms of action of therapeutic interventions and to identify non-responders to a specific treatment prior to the clinical endpoint. The results underscore the causal relevance of monocyte responses in the pathophysiology of severe COVID-19.[18,30]

Dexamethasone treatment response is reflected in the epigenome of CD14^{+} monocytes early after treatment initiation

To investigate whether the observed differences in the dexamethasone treatment response on the transcriptional level are reflected by epigenetic profiles in monocytes, we selected patients with supplemental oxygen but without invasive mechanical ventilation at treatment start (World Health Organization (WHO) score of 4–5) and generated genome-wide DNA methylation profiles of blood samples at an earlier stage of treatment (median 2 days after initiation of dexamethasone treatment) than for the transcriptome analysis (median of 8 days) (Figure 4A). Patients were matched in pairs according to clinical status at treatment initiation and classified based on their future WHO score (median 9 days later) as either dexamethasone non-responders (increased WHO score, i.e., clinical deterioration to intubation and invasive mechanical ventilation, need for additional organ replacement, or death) or dexamethasone responders (stable or improved clinical status and WHO score). DNA methylation profiles of fluorescence-activated cell sorting

Figure 3. Dexamethasone-induced transcriptional modulation of monocytes is linked to clinical outcome

(A) Percentages of Dexa response monocyte state of all monocytes stratified by severity and treatment with each dot representing one donor. Statistical testing using Wilcoxon test, resulting p values are indicated.

(B) Monocyte relative cluster distribution from CyTOF analysis for cluster 3 (CD14^{+}CD16^{-}CD163^{hi}, clustering see Figure S3B). Wilcoxon test for statistical testing, and resulting p values are indicated.

(C) Mean scaled signal intensity of CD163 in myeloid cells (CyTOF) by treatment group and severity. Wilcoxon test for statistical testing, and resulting p values are indicated.

(D) Percentages of Dexa response monocyte state of all monocytes in severe patients with dexamethasone treatment stratified by outcome. Statistical testing using Wilcoxon test, and resulting p values are indicated.

(E) Volcano plot showing the differentially expressed genes (DEGs) for Dexa vs. control in severe COVID-19 survivors (DE parameters: $\log_2$FC = 0.25, min.pct = 0.1).

(F) Violin plots for a selection of genes from (E) belonging to the MHC class II, alarmins, or cytokines/chemokines group.

(G) Percentages of "*S100A*^{hi}" monocyte state of all monocytes stratified by outcome in dexamethasone-treated severe COVID-19 patients. Statistical testing using Wilcoxon test, and resulting p values are indicated.

(H) Volcano plot showing the DEG between severe COVID-19 patients treated with dexamethasone who survived vs. those who were treated but deceased in monocytes (DE parameters: $\log_2$FC = 0.25, min.pct = 0.1).

(I) Signature enrichment of the *HLA-DR*^{lo}*S100A*^{hi} monocytes from Schulte-Schrepping et al.[18] in monocytes of severe COVID-19 patients stratified by treatment and outcome.

(J) Enrichment of the Dexa response monocyte signature (n = 30) in both bronchoalveolar lavage (BAL) COVID-19 monocytes (left) and macrophages (right), cohort overview in Figure S3G. Statistical testing using the Wilcoxon test (alternative = "greater"), and resulting p values are indicated.

See also Figure S3.

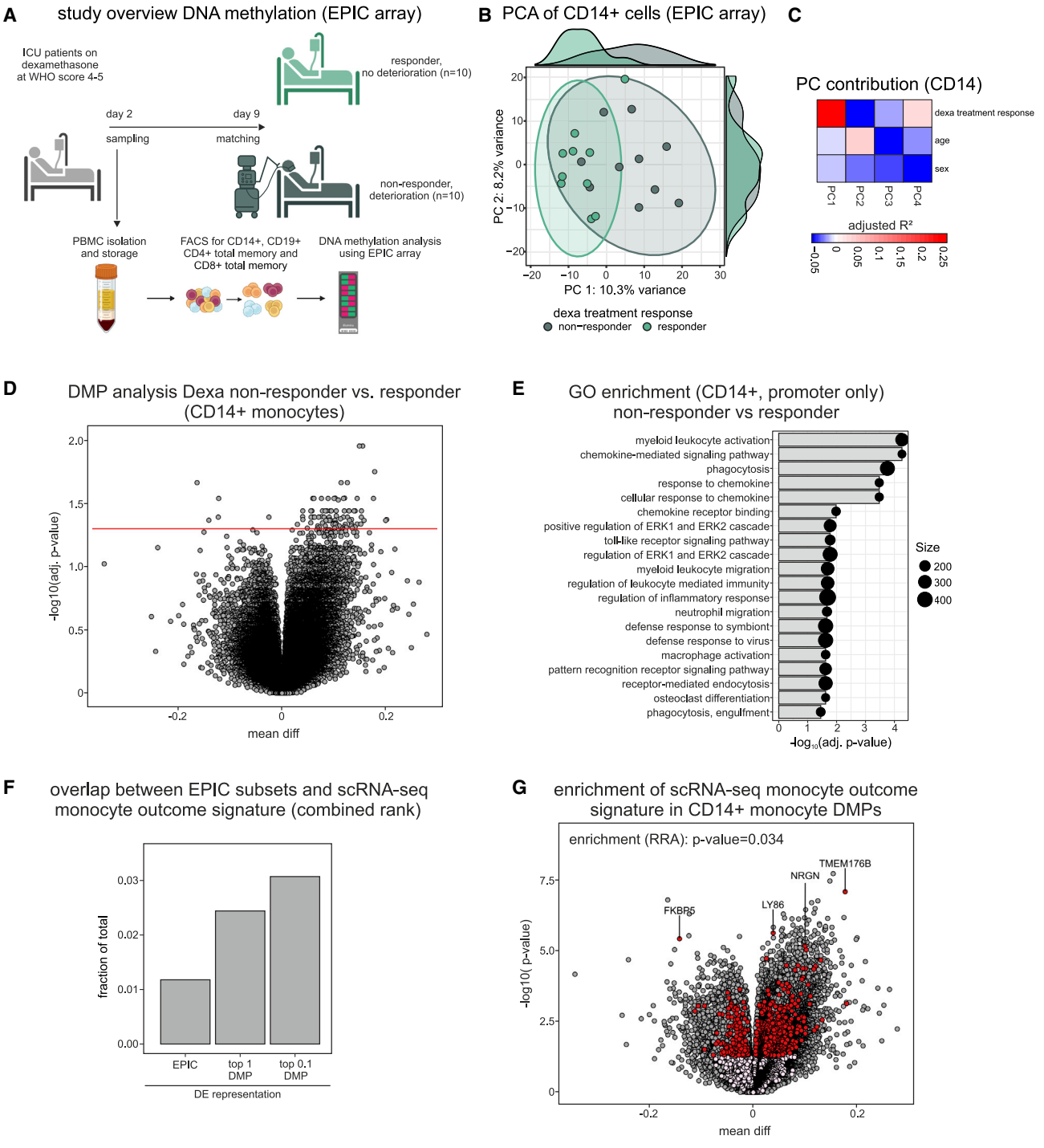

Figure 4. Treatment response is reflected in the epigenome of CD14⁺ monocytes early after treatment initiation

(A) Study design: PBMCs were isolated from patients (WHO score of 4–5 at dexamethasone treatment start) 1–4 days after the start of Dexa treatment. Ten matching pairs of treatment non-responders/responders were selected based on their increased/not-increased WHO score 5–11 days after Dexa treatment, respectively. $CD14^{+}CD16^{-}$ monocytes, $CD19^{+}$ B cells, $CD4^{+}$ memory T cells, and $CD8^{+}$ memory T cells were purified using flow cytometry (FACS) and analyzed on the Infinium MethylationEPIC BeadChip array for genome-wide DNA methylation.

(B) Principal-component analysis (PCA) was performed on the genome-wide DNA methylation datasets of $CD14^{+}$ monocytes. Histograms on the axes show the distribution of dexamethasone treatment response group samples.

(C) PC linear regression analysis of covariates. Contribution of dexamethasone treatment response, age, and sex are displayed for PCs 1–4.

(legend continued on next page)

(FACS)-purified CD14$^+$CD16$^-$ monocytes, CD19$^+$ B cells, CD4$^+$ memory T cells, and CD8$^+$ memory T cells (Figure S4A) showed the strongest differences by cell type without differentiating between responders and non-responders in the global principal-component analysis (PCA, Figure S4B). To define treatment response-related differences, each cell compartment was subsetted and analyzed individually. A separation between responders and non-responders was observed in the PCA for CD14$^+$ monocytes (Figure 4B), which was not seen in CD19$^+$ B cells or CD4$^+$ and CD8$^+$ memory T cells (Figure S4C). PC linear regression analysis of the CD14$^+$ monocytes confirmed the highest influence to be the dexamethasone treatment-response group on the first principal component (Figures 4B and 4C). To further explore the epigenetic differences within CD14$^+$ monocytes between non-responding and responding patients, we determined significantly differentially methylated positions (DMPs, Figure 4D). Functional enrichment analysis of promoter-associated DMPs revealed high association of GO terms such as "myeloid leukocyte activation," "response to chemokine," "myeloid leukocyte migration," and "regulation of inflammatory response," displaying epigenetic remodeling of promoter elements of genes contributing to a proinflammatory program in CD14$^+$ monocytes (Figure 4E).

Comparing these results to our findings on the transcriptome level (~8 days after treatment initiation), outcome-specific monocyte signature genes for severe dexamethasone-treated COVID-19 patients who deceased (Figure 3H) were overrepresented in the top 1% DMPs (based on combined rank) with an even stronger overrepresentation in the top 0.1% DMPs, indicating significant differential methylation changes in these signature genes (Figure 4F). This was supported by a significant robust rank aggregation (RRA) enrichment analysis (Figure 4G).

Taken together, we observed profound epigenetic differences in monocytes of dexamethasone non-responders vs. responders early after treatment initiation, thus preceding the observed transcriptional changes. Differences were mainly associated with a proinflammatory program and also showed enrichment of the outcome signature retrieved from single monocyte transcriptomes, further supporting the importance of this gene program to be targeted if dexamethasone therapy is to become clinically effective.

Dexamethasone-induced monocyte signatures enrich in whole blood transcriptomes of two clinical cohorts and stratify outcome

Given the clear outcome-associated transcriptional changes, particularly in the monocyte compartment, we next investigated whether these changes could be recapitulated in whole blood transcriptomes and whether transcriptome information from early time points after dexamethasone treatment initiation would be informative to stratify patients according to their clinical outcome.

To this end, we generated whole blood bulk transcriptomes from 92 patients of our single-center COVID-19 cohort (Charité, Pa-COVID-19), sampled at 4 days after treatment initiation (Figure 5A), 4 days earlier than for the scRNA-seq analysis. PCA revealed expression differences between moderately ill patients, severely ill patients who survived, and severely ill patients who later died (Figure 5B), indicating the feasibility to detect outcome-related differences from whole blood transcriptomes. We compiled two transcriptome signatures related to fatal outcome, i.e., for up- and downregulated transcripts, based on the single-cell monocyte transcriptomes (Figures 2 and 3). Enrichment scores for these signatures were calculated for each patient and integrated for each patient group. We observed significant disease severity- and outcome-dependent differences, with enrichment of the "deceased upregulated" signature in deceased patients and highest enrichment of the "deceased downregulated" signature in patients with the lowest disease severity (moderate COVID-19) (Figure S5A). These findings indicated that outcome-associated monocyte-specific gene signatures are detectable in whole blood transcriptomes, even at an earlier time point after treatment initiation (4 vs. 8 days), and that these signatures could stratify patients by outcome (Figure S5A).

Next, we utilized samples collected from 90 patients in a German multi-center cohort (CAPNETZ cohort) at an even earlier time point after initiation of dexamethasone treatment (2 vs. 4 days, Figure 5C). Also in this cohort, we identified differences between patients according to disease severity and outcome (moderate, severe survived, and severe deceased) by PCA (Figure 5D), albeit less clear than in the samples from the single-center cohort collected at a later time point of 4 days post treatment initiation. Accordingly, the single monocyte transcriptome-derived deceased upregulated signature was not significantly enriched, but the deceased downregulated signature enriched with statistically significant differences between the three groups (Figure S5B).

To assess the likelihood of obtaining an enrichment of the single monocyte transcriptome-derived signatures of that size with the respective significance, we performed a permutation test with 500 gene sets randomly drawn from each dataset, respectively, and calculated the enrichment scores in deceased and surviving patients. In contrast to the vast majority of these random gene sets, we observed a highly specific enrichment of our original single monocyte transcriptome-derived signatures in both cohorts, particularly of the deceased upregulated

(D) Volcano plot of differentially methylated positions (DMPs) in CD14$^+$ monocytes comparing both dexamethasone response groups. The red line indicates the false discovery rate (FDR) of 0.05 (Benjamini-Hochberg).
(E) Gene Ontology enrichment analysis performed on promoter-associated DMPs for CD14$^+$ monocytes comparing dexamethasone response groups.
(F) Fraction of outcome signature genes from monocytes (deceased vs. survivors, Figure 3H) within all samples on the EPIC array, the top 1% of DMPs (based on combined rank), and the top 0.1% of DMPs.
(G) Volcano plot with marked sites of monocyte outcome signature genes displaying differential methylation (red dots: p value < 0.05; pink dots: not significant). Gene names were displayed for DEG sites with an FDR < 0.05. Statistical significance of the overlap between differential DNA methylation and differential gene expression was calculated (robust rank aggregation [RRA], p value = 0.034).
See also Figure S4.

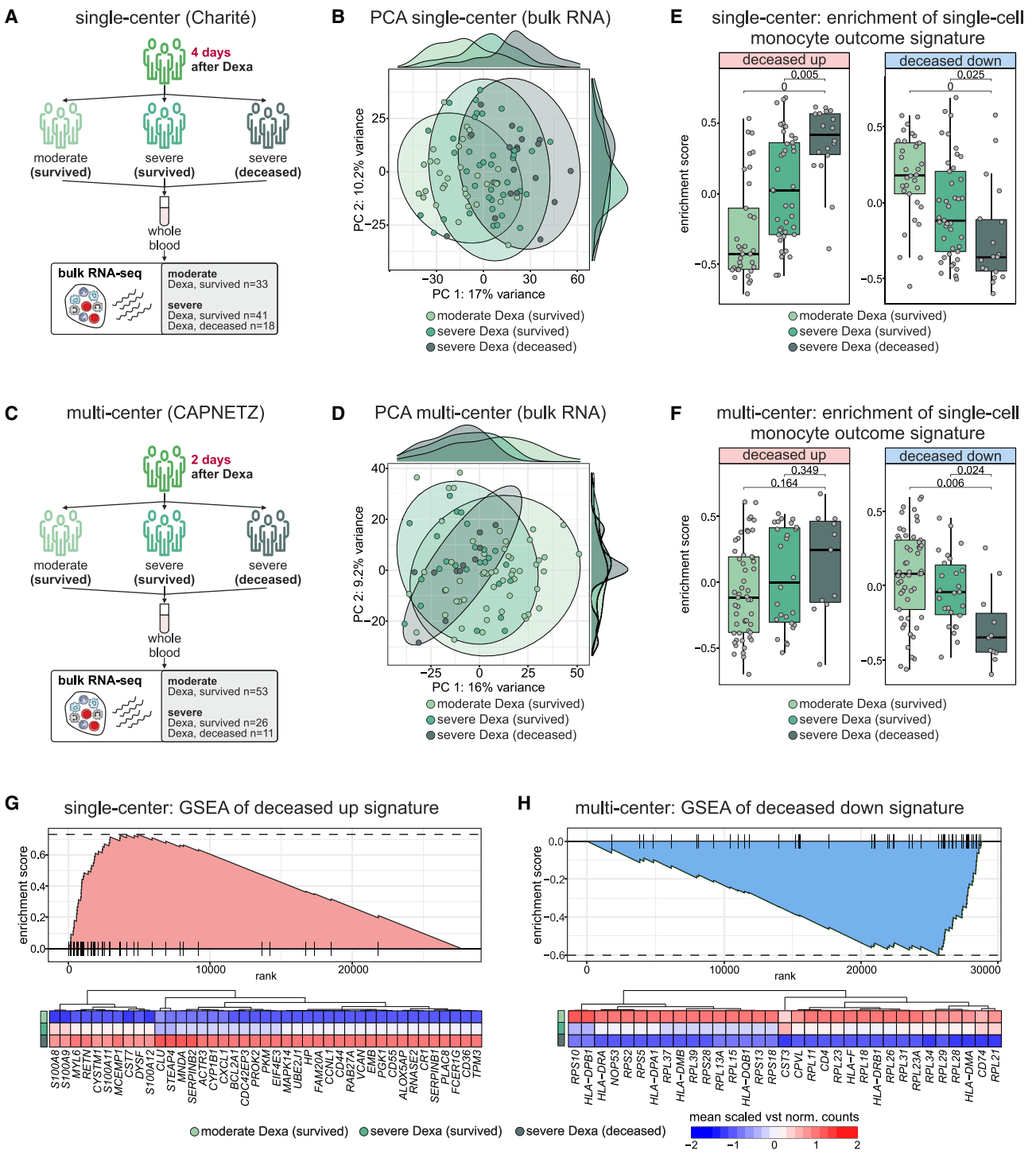

Figure 5. Monocyte-specific signatures enrich in whole blood transcriptomes of two validation cohorts and stratify outcome

(A) Schematic representation of the single-center (Charité) COVID-19 cohort used for whole blood transcriptome data analysis sampled on average at 4 days after dexamethasone treatment initiation. Included sample numbers are indicated.

(B) Principal-component analysis (PCA) plot showing the distribution of the top 5,000 most variable genes present in the single-center cohort, color-coded according to COVID-19 severity and outcome.

(C) Schematic representation of the multi-center (CAPNETZ) cohort used for whole blood transcriptome data analysis sampled on average 2 days after dexamethasone treatment initiation. Included sample numbers are indicated.

(legend continued on next page)

signature in the single-center cohort and of the deceased downregulated signature in the multi-center cohort. (Figures S5C and S5D.) To further increase the robustness of the enrichment analysis, we varied the number of genes to be included in the gene signature and optimized the signature size based on the calculated enrichment scores and different enrichment between the groups in both cohorts (Figures S5E and S5F). These optimized signatures showed a high robustness for stratifying patients according to disease severity and outcome in the two independent cohorts, at early time points after treatment initiation (Figures 5E and 5F). Investigation of the driving genes of the enrichment of the outcome-related signature (Figures 5G, 5H, S5G, and S5H) revealed that the leading edge of the GSEA included the chemokine *CXCL1* together with the alarmins *S100A8*, *S100A9*, *S100A11*, and *S100A12*, resembling the monocyte phenotype in patients with severe acute COVID-19 for the deceased upregulated signature in the original single-center cohort (Figure 5G) and that enrichment of the deceased downregulated signature in the deceased patients was strongly driven by many MHC class II genes (Figure S5G). In the whole blood transcriptomes of the multi-center cohort sampled at 2 days post treatment initiation, the leading edge of the enrichment of the deceased upregulated signature did not yet contain the complete signature at this early time point in patients who later died, but already showed changes in *S100A12* and *CXCL1* (Figure S5H). Yet, the edge of the deceased downregulated signature was already enriched in MHC class II genes such as *CD74*, *HLA-DQB1*, *HLA-DRB1*, and *HLA-DRA* for patients who later died (Figure 5H). These results further emphasize the role of dexamethasone in reversing the severe acute COVID-19 phenotype, as early as 2 days after initiation of treatment.

Taken together, clinical outcome-related single monocyte transcriptome-based gene signatures derived from COVID-19 patients on average 8 days after initiation of dexamethasone treatment were enriched in whole blood bulk transcriptomes obtained at day 4 post treatment initiation and accurately stratified patients according to disease severity and outcome. In whole blood transcriptomes collected 2 days after treatment initiation in an independent cohort, we could only detect an enrichment of the gene signature based on downregulated genes, indicating that dexamethasone treatment effects become apparent in whole blood transcriptomes between 2 and 4 days after treatment initiation.

The results demonstrate the versatility of single-cell sequencing of clinical samples to reveal *in vivo* effects of pharmacological treatment and that gene signatures derived from these analyses can be applied to larger clinical cohorts to stratify study patients by outcome, even at early time points after treatment initiation.

DISCUSSION

GCs are among the most widely prescribed drugs worldwide and a cornerstone for the treatment of a variety of acute and chronic inflammatory conditions. In clinical practice, they are often regarded as effective yet rather nonspecific immunosuppressants, despite an established molecular understanding that both naturally occurring and pharmacologically designed GCs are acting via specific binding to GC receptors.[31,32] Responsiveness to GC treatment is known to be heterogeneous among patients, possibly influenced by the variety of diverse GC receptor isoforms, which mediate their differential genomic and non-genomic effects.[26,33]

To better understand the specificity and the molecular mode of action of GC treatment in COVID-19, we applied high-content bulk transcriptomics and high-resolution single-cell technologies in two clinical cohorts of patients with COVID-19. We provide evidence that dexamethasone treatment in severe COVID-19 leads to a highly specific immune modulation. Major changes of molecular phenotypes occur mainly in the myeloid cell compartment, where dexamethasone elicits a treatment-specific cell state in a fraction of monocytes, with induction of genes with well-known regulatory functions including cell surface receptors, transcriptional regulators, and translational regulators, while many chemokines and *IL-1B* are decreased in expression. Defining qualitative and quantitative effects of dexamethasone treatment on the cellular and molecular level supported a specific immunomodulatory effect, with many changes induced irrespective of disease severity. Importantly, these effects are reminiscent of changes described previously in other therapeutic settings, such as rheumatoid arthritis, inflammatory bowel diseases, or allergic asthma,[32] for example, the increase of expression of certain genes with regulatory function including Thrombospondin 1 (*THBS1*), *IL1R2*, or GC-induced leucine zipper protein GILZ (*TSC22D3*). Functional enrichment across cell types pointed toward strong interference with NF-κB signaling, which is one of the well-known mechanisms downstream of GC receptor signaling.[21,22]

(D) PCA illustrating the distribution of the top 5,000 most variable genes present in the multi-center cohort, color-coded according to COVID-19 severity and outcome.

(E) Boxplots displaying the gene set variation analysis (GSVA) enrichment scores of the optimized deceased upregulated signature (left plot) and deceased downregulated signature (right plot) in the single-center cohort, split and colored by the COVID-19 severity status and outcome. Wilcoxon test and Benjamini-Hochberg adjustment were utilized for statistical analysis.

(F) Boxplots displaying the GSVA enrichment scores of the optimized deceased upregulated signature (left plot) and deceased downregulated signature (right plot) in the multi-center cohort, split and colored by the COVID-19 severity status and outcome. Wilcoxon test and Benjamini-Hochberg adjustment were utilized for statistical analysis.

(G) Gene set enrichment analysis (GSEA) of the optimized deceased upregulated signature in the deceased patient group of the Charité cohort. Ranking of samples is based on expression-level statistics, and the running sum is visualized. The heatmap depicts the scaled variance-stabilized mean expression per COVID-19 severity status and outcome of the genes included in the leading edge.

(H) GSEA of the optimized deceased downregulated signature in the deceased patient group of the multi-center cohort. Ranking of samples is based on expression-level statistics, and the running sum is visualized. The heatmap depicts the scaled batch-corrected variance-stabilized mean expression per COVID-19 severity status and outcome of the genes included in the leading edge.

See also Figure S5.

Most strikingly, the molecular response to dexamethasone was linked to clinical treatment response and outcome, as the previously described dysfunctional molecular phenotype associated with severe acute COVID-19 (*HLA-DR*^{lo}*S100A*^{hi} monocytes)[18] was reversed in patients surviving severe COVID-19. This illustrates that dexamethasone therapy in this clinical situation is not only immunosuppressive but rather immunomodulatory since expression of genes related to effective immune function was re-established. In fact, a specific Dexa response state within monocytes, uncovered by single-cell transcriptome analysis, revealed that not all monocytes respond to treatment. Patients succumbing to the disease did not show a reversal of the dysfunctional molecular phenotype in the monocyte compartment (*HLA-DR*^{lo}*S100A*^{hi} monocytes), accompanied by a lack of the dexamethasone response monocyte cell state in most of these patients.

The dexamethasone response signature from blood monocytes also enriched in monocytes and macrophages from BAL samples of dexamethasone-treated survivors, but not of treated non-survivors or GC-naive patients of our cohort. The role of inflammatory and potentially profibrotic monocytes and monocyte-derived macrophages for the development of acute respiratory distress syndrome (ARDS) in COVID-19 has been documented in numerous studies.[34] The reversal of the dysfunctional molecular phenotype of monocytes in the lung, associated with dexamethasone treatment and positive outcome (survival), links our findings in circulating immune cells to dexamethasone treatment-induced protection.

The differences in transcriptional changes following treatment were preceded by epigenetic changes in the proinflammatory program of CD14^{+} monocytes, which also differed between responders and non-responders. An outcome-related signature generated from the monocyte transcriptomes (8 days post treatment initiation) was successfully applied to whole blood transcriptomes sampled even earlier within two larger observational single-center and multi-center cohorts, respectively. The signature was enriched in whole blood transcriptomes from patients succumbing to COVID-19 in our single-center study already at 4 days post treatment initiation, indicating early treatment failure. Testing for generalizability of this potential predictor of treatment response and outcome in a national multi-center cohort at an even earlier time point revealed that more than 2 days of treatment are required for molecular outcome stratification.

Several attempts have been made to identify subgroups of patients with severe COVID-19 who are likely to respond differently to anti-inflammatory treatment. Two distinct groups of patients with COVID-related ARDS, similar to the previously described hypoinflammatory and hyperinflammatory ARDS subphenotypes,[35] were reported to show differential response to corticosteroid treatment[36] and have been proposed for a biomarker-guided corticosteroid dosing in COVID-19.[37] Similarly, peripheral blood transcriptomes have been used to identify two different endotypes of patients with severe COVID-19 based on IFN-related or checkpoint genes, who showed cluster-specific effects of corticosteroid treatment.[38] Attempts to identify different COVID-19 endotypes or phenotypes in terms of their response to anti-inflammatory treatment are particularly important in light of the fact that several clinical trials initially failed to demonstrate a clear survival benefit of corticosteroid treatment in COVID-19,[4,39] in addition to the fact that only about one-third of the mechanically ventilated severe COVID-19 patients benefit from dexamethasone therapy.[1] There is a long history of research investigating GC responsiveness,[40] based on the known heterogeneity in treatment response and the variety of unfavorable effects of corticosteroids, particularly associated with their long-term use. In asthma, distinct endotypes have been defined based on the level of type 2 inflammation, known to predict response to GC treatment.[41] Also in other clinical conditions, e.g., community-acquired pneumonia, the significance of steroid treatment is not fully evident, with clear signs that certain patient groups benefit more from adjunct corticosteroid treatment than others, thus emphasizing the importance of early patient stratification.[42,43] In our view, the approach presented in this study goes one step beyond molecular stratification and definition of disease endotypes by providing direct information on therapy response as a form of molecular therapy monitoring. The potential of whole blood transcriptome-based signatures to optimize dexamethasone treatment regimens should be evaluated in a prospective pivotal trial in the future.

Limitations of the study

Our analysis of the effects of dexamethasone treatment was based on a large prospective, single-center cohort study and an independent prospective, multi-center cohort study for validation of the transcriptional signature enrichment associated with fatal outcome. One important limitation of this approach is the fact that both cohorts were observational and not primarily designed to study the effect of dexamethasone treatment. However, we took advantage of the fact that dexamethasone treatment was only introduced into SOC in the second wave, thus allowing for a well-matched comparison of COVID-19 patients of similar demographics and disease severity, infected with the same viral variant (D614G), that differed only by treatment. Nonetheless, it would be preferable to conduct studies of this nature within the setting of randomized controlled trials, designed to study clinical endpoints as well as mechanisms of action of the investigated drugs. Thus, adaptive platform trials, such as the RECOVERY study, designed to rapidly test the effectiveness of repurposed drugs or new therapies in public health emergencies, would benefit from incorporating high-resolution biomarker studies to uncover mechanisms and to identify target and risk populations who would benefit most from the respective treatment or alternative therapies. To this end, global networks of specialized medical institutions capable of performing highly standardized, high-resolution methods on study samples at high throughput are needed to facilitate this accelerated treatment development. While our approach included well-matched cohorts, the study period was restricted to the early phase of the pandemic. This is a limitation since immunological and virological characteristics have changed during the course of the pandemic. Dexamethasone remains the SOC for patients with moderate to severe COVID-19, yet, it is unknown whether it is still equally effective in re- and breakthrough infections. The use of corticosteroids in other respiratory infections has been controversial, with potentially detrimental effects in influenza infections and mixed results in community-acquired pneumonia. However, it will be difficult to generate new data since it would not be

ethical to withhold dexamethasone in patients with severe COVID-19.

Our study has several implications. First, GC treatment in acute COVID-19 is better characterized as an immunomodulatory rather than immunosuppressive therapy. Second, early outcome predictors could guide personalized therapy by identifying patients not responding adequately to GCs, necessitating early addition of other immunomodulators such as Janus kinase inhibitors or IL-6 receptor blockers.[44] As high-dose GC therapy has been reported to increase mortality in hypoxic moderate to severe patients not requiring mechanical ventilation,[6] prolonged dexamethasone treatment in severe COVID-19 patients might also increase the risk for secondary infections[45] and thereby might contribute to reduced survival rates in this subgroup of patients.[46] Third, a more precise use of GCs in other medical conditions would be highly desirable, and a more precise stratification could be achieved based on clinical trials that incorporate single-cell resolution biomarker studies.

Taken together, we provide single-cell-level resolved molecular phenotype information for the immunomodulatory effect of dexamethasone treatment in patients with COVID-19, which could be utilized for clinical decision-making regarding therapy reevaluation for dexamethasone treatment in the future. Combined with transcriptome-based reverse drug target prediction approaches and randomized controlled trials, this approach can form the basis for faster drug repurposing solutions for future emerging infectious diseases, and it may even be a blueprint for the development of precision medicine for other infectious and non-infectious diseases.

STAR★METHODS

Detailed methods are provided in the online version of this paper and include the following:

- KEY RESOURCES TABLE
- RESOURCE AVAILABILITY
  - Lead contact
  - Materials availability
  - Data and code availability
- EXPERIMENTAL MODEL AND STUDY PARTICIPANT DETAILS
  - Patient cohorts and study flow overview
  - Single-cell transcriptomics, CyTOF, and FACS
  - Subject details blood sc transcriptomics subgroup
  - Subject details FACS subgroup
  - Subject details CyTOF subgroup
  - Subject details BAL sc-transcriptomics subgroup
  - Epigenetics
  - Subject details epigenetics
  - Bulk transcriptomics
  - Subject details single-center bulk subgroup
  - Subject details multi-center bulk subgroup
  - Ethics
- METHOD DETAILS
  - Details for blood single-cell transcriptomics
  - Details for DNA methylation
  - Details for CyTOF
  - Details for bulk transcriptomics
  - BAL single-cell processing and sequencing
  - Monocyte FACS verification
  - SARS-CoV-2 spike protein ELISA
- QUANTIFICATION AND STATISTICAL ANALYSIS
  - Analysis of blood single-cell transcriptome data
  - Analysis of BAL single-cell transcriptome data
  - Bulk RNA-sequencing analysis
  - CyTOF: Cell identification and cluster analysis
  - Analysis of DNA methylation data
  - Enrichment analysis for DNA methylation data
  - Data visualization

SUPPLEMENTAL INFORMATION

Supplemental information can be found online at https://doi.org/10.1016/j.cell.2024.06.014.

CONSORTIA

Pa-COVID-19 Study Group

Stefan Hippenstiel, Saskia Zvorc, Christof von Kalle, Mirja Mittermaier, Fridolin Steinbeis, Tilman Lingscheid, Bettina Temmesfeld-Wollbrück, Thomas Zoller, Holger Müller-Redetzky, Alexander Uhrig, Daniel Grund, Miriam S. Stegemann, Katrin M. Heim, Ralf H. Hübner, Bastian Opitz, Kai-Uwe Eckardt, Martin Möckel, Victor Corman, Felix Balzer, Claudia Spies, Steffen Weber-Carstens, Chantip Dang-Heine, Michael Hummel, Georg Schwanitz, Uwe D. Behrens, Maria Rönnefarth, Sein Schmidt, Linda Jürgens, Sophy Denker, Moritz Pfeiffer, Luisa Mrziglod, Felix Machleidt, Sebastian Albus, Felix Bremer, Jan-Moritz Doehn, Tim Andermann, Carmen Garcia, Philipp Knape, Philipp M. Krause, Liron Lechtenberg, Yaosi Li, Panagiotis Pergantis, Till Jacobi, Teresa Ritter, Berna Yedikat, Lennart Pfannkuch, Christian Zobel, Ute Kellermann, Susanne Fieberg, Laure Bosquillon de Jarcy, Anne Wetzel, Michael Ney, Simon Ronicke, Maria Roth, Christoph Tabeling, Moritz Müller-Plathe, Jan M. Kruse, Daniel Zickler, Andreas Edel, Gianluca Barbone, Marius Eckart, Martin Kluge, Tobias Püngel, Münevver Demir, Robert Röhle, Theresa Keller, Christoph Jochum, Britta Stier, Roland Körner, Nils B. Mueller, Stefan Schaller, Viktor Wegener, Lucie Kretzler, Lil A. Meyer-Arndt, Linna Li, Isabelle Wirsching, Denise Treue, Dana Briesemeister, Jenny Schlesinger, Lara Bardtke, Kai Pohl, Daniel Wendisch, Anna L. Hiller, Sophia Brumhard, Marie Luisa Schmidt, Leonie Meiners, and Patricia Tscheak and all study nurses.

CAPNETZ Study Group except the authors

A. Fuchs, M. Engelmann (Augsburg); D. Stolz (Basel/Freiburg); W. Bauer, H.C. Mücke (Berlin); S. Schmager (Cottbus); B. Schaaf, J. Kremling, D. Nickoleit-Bitzenberger, H. Azzaui, M. Hower, F. Hempel, K. Prebeg, K. Popkirova (Dortmund); M. Kolditz(Dresden); C. Bellinghausen, A. Grünewaldt (Frankfurt), M. Panning (Freiburg); T. Welte, T. Fühner, M. van't Klooster, G. Barten-Neiner, W. Kröner, O. Unruh, N. Adaskina, F. Eberhardt, C. Julius, T. Illig, N. Klopp (Hannover); M. Pletz, B.T. Schleenvoigt, C. Forstner, A. Moeser, J. Ankert (Jena); D. Drömann, P. Parschke, K. Franzen, J. Rupp, N. Käding, F. Waldeck (Lübeck); C. Spinner, J. Erber, F. Voit, J. Schneider (Munich); D. Heigener, I. Hering (Rotenburg/Wümme); W. Albrich, M. Seneghini, F. Rassouli, S. Baldesberger (St. Gallen); A. Essig, S. Stenger, M. Wallner (Ulm); H. Burgmann, L. Traby, L. Schubert, R. Chen (Vienna); and all study nurses.

ACKNOWLEDGMENTS

We thank all the patients who have participated in the study and donated their blood. We thank Anne Schulze for expert technical assistance; Gilles Gasparoni for sharing protocols; Olesya Unruh, Grit Barten, and Frank Eberhardt from CAPNETZ for assistance during provision of samples and data; BIH Flow & Mass Cytometry Core facility for flow-cytometric cell sorting; the German Cancer Consortium (DKTK), Site Berlin (AG Capper) for access to the iScan instrument; and Sach Mukherjee for critical discussion of the manuscript.

K.D. is supported by the DFG via HA 6409/5-1. C.T. is a participant in the BIH Charité Clinician Scientist Program funded by the Charité-Universitätsmedizin and the Berlin Institute of Health at Charité (BIH). F.T. has received funding

from Allergan for a COVID-19-related IIT. N.S. reports grants from the German Research Foundation (SFB-TR84 C09) and from the German Ministry of Education and Research (BMBF) in the framework of CAPSyS (01ZX1604B and 01ZX1304B). A.-E.S. and O.D. thank the DFG – GRK2157 for support. A.-E.S. thanks FOR-COVID initiative funded by the Bayerisches Staatsministerium für Wissenschaft und Kunst. This work was supported by the Stiftung Charité to J.K.P. CAPNETZ was founded by a BMBF grant (FKZ 01KI07145) 2001–2011 and has been an associated member of the German Center for Lung Research (FKZ 82DZL002B4) since 2013. B.S. is supported by the German Research Foundation (DFG) via the SFB 1444 - project #427826188 and by the German Federal Ministry of Education and Research (BMBF) via FKZ 01IK20337 - RECAST; FKZ 01KX2021 - COVIM; FKZ 01EP2201 – NKSG; and FKZ 01KX2121 – NAPKON TIP. J.L.S. is supported by the DFG via the GRK2168 – #272482170, BMBF-funded project iTREAT (01ZX2202B), and Helmholtz-funded project sparse2big (ZT-I-0007). A.C.A., M.B., and J.L.S. are members of the excellence cluster ImmunoSensation (EXC 2151) funded by the German Research Foundation (DFG) under grant agreement #390873048 and are supported by the DFG via the SFB 1454 – project number #432325352, grant #466168337, and grant #466168626; the BMBF-funded project IMMME (01EJ2204D) and National Clinical Study Group (NKSG) (FKZ 01EP2201); and the EU-funded project ImmunoSep (#847422) and NEUROCOV, receiving funding from the RIA HORIZON Research and Innovation under GA No. 101057775. A.C.A. is supported by the Deutsche Forschungsgemeinschaft (DFG, German Research Foundation) via grant #458854699. F.K. is supported by the German Ministry of Education and Research (BMBF) in the framework of CAP-TSD (031L0286B). L.E.S and F.K. are supported by the COVIM platform of Netzwerk Universitätsmedizin (01KX2021, 01KX2121) and by the German Federal Institute for Dugs and Medical Devices (V-2021.3 / 1503_68403 / 2021–2022).

AUTHOR CONTRIBUTIONS

Conceptualization: E.T.H., L.E.S., J.L.S., A.C.A., and F.K.; investigation: R.K., E.T.H., K.D., O.B., F.H., O.D., M.v.U., S.M., L.B., J.S.-S., L.P., B.K., M.K., S.B., H.T., G.H., E.D.D., J.N., M.D.B., P.G., and J.T.; resources: E.T.H., P.S., C.T., P.G., L.L., B.M.P.-L., F.T., G.R., N.S., and M.W., CAPNETZ Study Group, Pa-COVID-19 study group, A.-E.S., J.K.P., B.S., L.E.S., J.L.S., A.C.A., and F.K.; data curation: R.K., E.T.H., D.H., P.T.L., K.D., O.B., F.H., O.D., M.v.U., P.S., C.T., and C.L.; data analysis: R.K., E.T.H., K.D., O.B., F.H., L.B., J.S.-S., L.P., B.K., M.B., T.U., and A.-E.S.; visualization: R.K., K.D., O.B., F.H., O.D., and L.P.; writing – original draft: R.K., E.T.H., K.D., F.H., J.K.P., B.S., L.E.S., J.L.S., A.C.A., and F.K.; writing – review & editing: R.K., E.T.H., K.D., F.H., P.S., C.T., A.E.S., J.K.P., L.E.S., J.L.S., A.C.A., and F.K.

DECLARATION OF INTERESTS

The authors declare no competing interests.

Received: July 24, 2023
Revised: February 27, 2024
Accepted: June 10, 2024
Published: July 3, 2024

REFERENCES

1. RECOVERY Collaborative Group, Horby, P., Lim, W.S., Emberson, J.R., Mafham, M., Bell, J.L., Linsell, L., Staplin, N., Brightling, C., Ustianowski, A., et al. (2021). Dexamethasone in Hospitalized Patients with Covid-19. N. Engl. J. Med. *384*, 693–704. https://doi.org/10.1056/NEJMoa2021436.
2. Aschenbrenner, A.C., Mouktaroudi, M., Krämer, B., Oestreich, M., Antonakos, N., Nuesch-Germano, M., Gkizeli, K., Bonaguro, L., Reusch, N., Baßler, K., et al. (2021). Disease severity-specific neutrophil signatures in blood transcriptomes stratify COVID-19 patients. Genome Med. *13*, 7. https://doi.org/10.1186/s13073-020-00823-5.
3. WHO Rapid Evidence Appraisal for COVID-19 Therapies (REACT) Working Group, Sterne, J.A.C., Murthy, S., Diaz, J.V., Slutsky, A.S., Villar, J., Angus, D.C., Annane, D., Azevedo, L.C.P., Berwanger, O., et al. (2020). Association Between Administration of Systemic Corticosteroids and Mortality Among Critically Ill Patients With COVID-19: a Meta-analysis. JAMA *324*, 1330–1341. https://doi.org/10.1001/jama.2020.17023.
4. Tomazini, B.M., Maia, I.S., Cavalcanti, A.B., Berwanger, O., Rosa, R.G., Veiga, V.C., Avezum, A., Lopes, R.D., Bueno, F.R., Silva, M.V.A.O., et al. (2020). Effect of Dexamethasone on Days Alive and Ventilator-Free in Patients With Moderate or Severe Acute Respiratory Distress Syndrome and COVID-19: The CoDEX Randomized Clinical Trial. JAMA *324*, 1307–1316. https://doi.org/10.1001/jama.2020.17021.
5. National Institutes of Health. National Institutes of Health COVID-19 Treatment Guidelines Panel. Coronavirus Disease 2019 (COVID-19) Treatment Guidelines. https://www.covid19treatmentguidelines.nih.gov/.
6. RECOVERY Collaborative Group. Electronic address: recoverytrial@ndph.ox.ac.uk; RECOVERY; Collaborative Group (2023). Higher dose corticosteroids in patients admitted to hospital with COVID-19 who are hypoxic but not requiring ventilatory support (RECOVERY): a randomised, controlled, open-label, platform trial. Lancet *401*, 1499–1507. https://doi.org/10.1016/S0140-6736(23)00510-X.
7. Les, I., Loureiro-Amigo, J., Capdevila, F., Oriol, I., Elejalde, I., Aranda-Lobo, J., Modesto, J., Güell-Farré, E., García, R., Murgadella-Sancho, A., et al. (2022). Methylprednisolone Pulses in Hospitalized COVID-19 Patients Without Respiratory Failure: A Randomized Controlled Trial. Front. Med. (Lausanne) *9*, 807981. https://doi.org/10.3389/fmed.2022.807981.
8. Thibeault, C., Bardtke, L., Vanshylla, K., di Cristanziano, V., Eberhardt, K.A., Stubbemann, P., Hillus, D., Tober-Lau, P., Mukherjee, P., Münn, F., et al. (2023). Short- and long-term T cell and antibody responses following dexamethasone treatment in COVID-19. JCI Insight *8*, e166711. https://doi.org/10.1172/jci.insight.166711.
9. Mühlemann, B., Thibeault, C., Hillus, D., Helbig, E.T., Lippert, L.J., Tober-Lau, P., Schwarz, T., Müller, M.A., Pa-COVID-19 collaborative study group, and Witzenrath, M., et al. (2021). Impact of dexamethasone on SARS-CoV-2 concentration kinetics and antibody response in hospitalized COVID-19 patients: results from a prospective observational study. Clin. Microbiol. Infect. *27*, 1520.e7–1520.e10. https://doi.org/10.1016/j.cmi.2021.06.008.
10. Arabi, Y.M., Mandourah, Y., Al-Hameed, F., Sindi, A.A., Almekhlafi, G.A., Hussein, M.A., Jose, J., Pinto, R., Al-Omari, A., Kharaba, A., et al. (2018). Corticosteroid Therapy for Critically Ill Patients with Middle East Respiratory Syndrome. Am. J. Respir. Crit. Care Med. *197*, 757–767. https://doi.org/10.1164/rccm.201706-1172OC.
11. Ni, Y.-N., Chen, G., Sun, J., Liang, B.-M., and Liang, Z.-A. (2019). The effect of corticosteroids on mortality of patients with influenza pneumonia: a systematic review and meta-analysis. Crit. Care *23*, 99. https://doi.org/10.1186/s13054-019-2395-8.
12. Sinha, S., Rosin, N.L., Arora, R., Labit, E., Jaffer, A., Cao, L., Farias, R., Nguyen, A.P., de Almeida, L.G.N., Dufour, A., et al. (2022). Dexamethasone modulates immature neutrophils and interferon programming in severe COVID-19. Nat. Med. *28*, 201–211. https://doi.org/10.1038/s41591-021-01576-3.
13. Wyler, E., Adler, J.M., Eschke, K., Teixeira Alves, G., Peidli, S., Pott, F., Kazmierski, J., Michalick, L., Kershaw, O., Bushe, J., et al. (2022). Key benefits of dexamethasone and antibody treatment in COVID-19 hamster models revealed by single-cell transcriptomics. Mol. Ther. *30*, 1952–1965. https://doi.org/10.1016/j.ymthe.2022.03.014.
14. Jeong, H.-W., Lee, J.S., Ko, J.-H., Hong, S., Oh, S.T., Choi, S., Peck, K.R., Yang, J.H., Chung, S., Kim, S.-H., et al. (2023). Corticosteroids reduce pathologic interferon responses by downregulating STAT1 in patients with high-risk COVID-19. Exp. Mol. Med. *55*, 653–664. https://doi.org/10.1038/s12276-023-00964-8.
15. Mazer, M.B., Davitt, E., Turnbull, I.R., Caldwell, C.C., Brakenridge, S.C., Remy, K.E., and Hotchkiss, R.S. (2021). In vitro-Administered Dexamethasone Suppresses T Cell Function With Reversal by Interleukin-7 in

Coronavirus Disease 2019. Crit. Care Explor. *3*, e0378. https://doi.org/10.1097/CCE.0000000000000378.

16. Wong, C.K.H., Lau, K.T.K., Au, I.C.H., Xiong, X., Chung, M.S.H., Leung, B.Y.C., Lau, E.H.Y., and Cowling, B.J. (2022). Initiation of Tocilizumab or Baricitinib Were Associated With Comparable Clinical Outcomes Among Patients Hospitalized With COVID-19 and Treated With Dexamethasone. Front. Pharmacol. *13*, 866441. https://doi.org/10.3389/fphar.2022.866441.
17. Kurth, F., Roennefarth, M., Thibeault, C., Corman, V.M., Müller-Redetzky, H., Mittermaier, M., Ruwwe-Glösenkamp, C., Heim, K.M., Krannich, A., Zvorc, S., et al. (2020). Studying the pathophysiology of coronavirus disease 2019: a protocol for the Berlin prospective COVID-19 patient cohort (Pa-COVID-19). Infection *48*, 619–626. https://doi.org/10.1007/s15010-020-01464-x.
18. Schulte-Schrepping, J., Reusch, N., Paclik, D., Baßler, K., Schlickeiser, S., Zhang, B., Krämer, B., Krammer, T., Brumhard, S., Bonaguro, L., et al. (2020). Severe COVID-19 Is Marked by a Dysregulated Myeloid Cell Compartment. Cell *182*, 1419–1440.e23. https://doi.org/10.1016/j.cell.2020.08.001.
19. D'Adamio, F., Zollo, O., Moraca, R., Ayroldi, E., Bruscoli, S., Bartoli, A., Cannarile, L., Migliorati, G., and Riccardi, C. (1997). A new dexamethasone-induced gene of the leucine zipper family protects T lymphocytes from TCR/CD3-activated cell death. Immunity *7*, 803–812. https://doi.org/10.1016/s1074-7613(00)80398-2.
20. Wang, Z., Rong, Y.P., Malone, M.H., Davis, M.C., Zhong, F., and Distelhorst, C.W. (2006). Thioredoxin-interacting protein (txnip) is a glucocorticoid-regulated primary response gene involved in mediating glucocorticoid-induced apoptosis. Oncogene *25*, 1903–1913. https://doi.org/10.1038/sj.onc.1209218.
21. Auphan, N., DiDonato, J.A., Rosette, C., Helmberg, A., and Karin, M. (1995). Immunosuppression by glucocorticoids: inhibition of NF-kappa B activity through induction of I kappa B synthesis. Science *270*, 286–290. https://doi.org/10.1126/science.270.5234.286.
22. Petta, I., Dejager, L., Ballegeer, M., Lievens, S., Tavernier, J., De Bosscher, K., and Libert, C. (2016). The interactome of the glucocorticoid receptor and its influence on the actions of glucocorticoids in combatting inflammatory and infectious diseases. Microbiol. Mol. Biol. Rev. *80*, 495–522. https://doi.org/10.1128/MMBR.00064-15.
23. Ehrchen, J.M., Roth, J., and Barczyk-Kahlert, K. (2019). More than suppression: glucocorticoid action on monocytes and macrophages. Front. Immunol. *10*, 2028. https://doi.org/10.3389/fimmu.2019.02028.
24. Ehrchen, J., Steinmüller, L., Barczyk, K., Tenbrock, K., Nacken, W., Eisenacher, M., Nordhues, U., Sorg, C., Sunderkötter, C., and Roth, J. (2007). Glucocorticoids induce differentiation of a specifically activated, anti-inflammatory subtype of human monocytes. Blood *109*, 1265–1274. https://doi.org/10.1182/blood-2006-02-001115.
25. Reddy, T.E., Pauli, F., Sprouse, R.O., Neff, N.F., Newberry, K.M., Garabedian, M.J., and Myers, R.M. (2009). Genomic determination of the glucocorticoid response reveals unexpected mechanisms of gene regulation. Genome Res. *19*, 2163–2171. https://doi.org/10.1101/gr.097022.109.
26. Wang, C., Nanni, L., Novakovic, B., Megchelenbrink, W., Kuznetsova, T., Stunnenberg, H.G., Ceri, S., and Logie, C. (2019). Extensive epigenomic integration of the glucocorticoid response in primary human monocytes and in vitro derived macrophages. Sci. Rep. *9*, 2772. https://doi.org/10.1038/s41598-019-39395-9.
27. Zannas, A.S., Wiechmann, T., Gassen, N.C., and Binder, E.B. (2016). Gene-Stress-Epigenetic Regulation of FKBP5: Clinical and Translational Implications. Neuropsychopharmacology *41*, 261–274. https://doi.org/10.1038/npp.2015.235.
28. Duhalde Vega, M., Olivera, D., Gastão Davanzo, G., Bertullo, M., Noya, V., Fabiano de Souza, G., Primon Muraro, S., Castro, I., Arévalo, A.P., Crispo, M., et al. (2022). PD-1/PD-L1 blockade abrogates a dysfunctional innate-adaptive immune axis in critical β-coronavirus disease. Sci. Adv. *8*, eabn6545. https://doi.org/10.1126/sciadv.abn6545.
29. Liao, M., Liu, Y., Yuan, J., Wen, Y., Xu, G., Zhao, J., Cheng, L., Li, J., Wang, X., Wang, F., et al. (2020). Single-cell landscape of bronchoalveolar immune cells in patients with COVID-19. Nat. Med. *26*, 842–844. https://doi.org/10.1038/s41591-020-0901-9.
30. Wendisch, D., Dietrich, O., Mari, T., von Stillfried, S., Ibarra, I.L., Mittermaier, M., Mache, C., Chua, R.L., Knoll, R., Timm, S., et al. (2021). SARS-CoV-2 infection triggers profibrotic macrophage responses and lung fibrosis. Cell *184*, 6243–6261.e27. https://doi.org/10.1016/j.cell.2021.11.033.
31. Buttgereit, F., Burmester, G.-R., and Lipworth, B.J. (2005). Optimised glucocorticoid therapy: the sharpening of an old spear. Lancet *365*, 801–803. https://doi.org/10.1016/S0140-6736(05)17989-6.
32. Reichardt, S.D., Amouret, A., Muzzi, C., Vettorazzi, S., Tuckermann, J.P., Lühder, F., and Reichardt, H.M. (2021). The role of glucocorticoids in inflammatory diseases. Cells *10*, 2921. https://doi.org/10.3390/cells10112921.
33. Ramamoorthy, S., and Cidlowski, J.A. (2016). Corticosteroids: mechanisms of action in health and disease. Rheum. Dis. Clin. North Am. *42*, 15–31,vii. https://doi.org/10.1016/j.rdc.2015.08.002.
34. Chen, S.T., Park, M.D., Del Valle, D.M., Buckup, M., Tabachnikova, A., Thompson, R.C., Simons, N.W., Mouskas, K., Lee, B., Geanon, D., et al. (2022). A shift in lung macrophage composition is associated with COVID-19 severity and recovery. Sci. Transl. Med. *14*, eabn5168. https://doi.org/10.1126/scitranslmed.abn5168.
35. Calfee, C.S., Delucchi, K., Parsons, P.E., Thompson, B.T., Ware, L.B., and Matthay, M.A.; NHLBI ARDS Network (2014). Subphenotypes in acute respiratory distress syndrome: latent class analysis of data from two randomised controlled trials. Lancet Respir. Med. *2*, 611–620. https://doi.org/10.1016/S2213-2600(14)70097-9.
36. Sinha, P., Furfaro, D., Cummings, M.J., Abrams, D., Delucchi, K., Maddali, M.V., He, J., Thompson, A., Murn, M., Fountain, J., et al. (2021). Latent Class Analysis Reveals COVID-19-related Acute Respiratory Distress Syndrome Subgroups with Differential Responses to Corticosteroids. Am. J. Respir. Crit. Care Med. *204*, 1274–1285. https://doi.org/10.1164/rccm.202105-1302OC.
37. Odeyemi, Y.E., Chalmers, S.J., Barreto, E.F., Jentzer, J.C., Gajic, O., and Yadav, H. (2022). Early, biomarker-guided steroid dosing in COVID-19 Pneumonia: a pilot randomized controlled trial. Crit. Care *26*, 9. https://doi.org/10.1186/s13054-021-03873-2.
38. López-Martínez, C., Martín-Vicente, P., Gómez de Oña, J., López-Alonso, I., Gil-Peña, H., Cuesta-Llavona, E., Fernández-Rodríguez, M., Crespo, I., Salgado Del Riego, E., Rodríguez-García, R., et al. (2023). Transcriptomic clustering of critically ill COVID-19 patients. Eur. Respir. J. *61*, 2200592. https://doi.org/10.1183/13993003.00592-2022.
39. Dequin, P.-F., Heming, N., Meziani, F., Plantefève, G., Voiriot, G., Badié, J., François, B., Aubron, C., Ricard, J.-D., Ehrmann, S., et al. (2020). Effect of Hydrocortisone on 21-Day Mortality or Respiratory Support Among Critically Ill Patients With COVID-19: A Randomized Clinical Trial. JAMA *324*, 1298–1306. https://doi.org/10.1001/jama.2020.16761.
40. Brown, H.M. (1958). Treatment of chronic asthma with prednisolone; significance of eosinophils in the sputum. Lancet *2*, 1245–1247. https://doi.org/10.1016/S0140-6736(58)91385-0.
41. Busse, W.W., Kraft, M., Rabe, K.F., Deniz, Y., Rowe, P.J., Ruddy, M., and Castro, M. (2021). Understanding the key issues in the treatment of uncontrolled persistent asthma with type 2 inflammation. Eur. Respir. J. *58*, 2003393. https://doi.org/10.1183/13993003.03393-2020.
42. Saleem, N., Kulkarni, A., Snow, T.A.C., Ambler, G., Singer, M., and Arulkumaran, N. (2023). Effect of Corticosteroids on Mortality and Clinical Cure in Community-Acquired Pneumonia: A Systematic Review, Meta-analysis, and Meta-regression of Randomized Control Trials. Chest *163*, 484–497. https://doi.org/10.1016/j.chest.2022.08.2229.
43. Dequin, P.-F., Meziani, F., Quenot, J.-P., Kamel, T., Ricard, J.-D., Badie, J., Reignier, J., Heming, N., Plantefève, G., Souweine, B., et al. (2023). Hydrocortisone in Severe Community-Acquired Pneumonia. N. Engl. J. Med. *388*, 1931–1941. https://doi.org/10.1056/NEJMoa2215145.

44. Ely, E.W., Ramanan, A.V., Kartman, C.E., de Bono, S., Liao, R., Piruzeli, M.L.B., Goldman, J.D., Saraiva, J.F.K., Chakladar, S., Marconi, V.C., et al. (2022). Efficacy and safety of baricitinib plus standard of care for the treatment of critically ill hospitalised adults with COVID-19 on invasive mechanical ventilation or extracorporeal membrane oxygenation: an exploratory, randomised, placebo-controlled trial. Lancet Respir. Med. *10*, 327–336. https://doi.org/10.1016/S2213-2600(22)00006-6.

45. Lingscheid, T., Lippert, L.J., Hillus, D., Kruis, T., Thibeault, C., Helbig, E.T., Tober-Lau, P., Pfäfflin, F., Müller-Redetzky, H., Witzenrath, M., et al. (2022). Characterization of antimicrobial use and co-infections among hospitalized patients with COVID-19: a prospective observational cohort study. Infection *50*, 1441–1452. https://doi.org/10.1007/s15010-022-01796-w.

46. Leistner, R., Schroeter, L., Adam, T., Poddubnyy, D., Stegemann, M., Siegmund, B., Maechler, F., Geffers, C., Schwab, F., Gastmeier, P., et al. (2022). Corticosteroids as risk factor for COVID-19-associated pulmonary aspergillosis in intensive care patients. Crit. Care *26*, 30. https://doi.org/10.1186/s13054-022-03902-8.

47. Dobin, A., Davis, C.A., Schlesinger, F., Drenkow, J., Zaleski, C., Jha, S., Batut, P., Chaisson, M., and Gingeras, T.R. (2013). STAR: ultrafast universal RNA-seq aligner. Bioinformatics *29*, 15–21. https://doi.org/10.1093/bioinformatics/bts635.

48. Martin, M. (2011). Cutadapt removes adapter sequences from high-throughput sequencing reads. EMBnet J. *17*, 10. https://doi.org/10.14806/ej.17.1.200.

49. Andrews S. FastQC: A Quality Control Tool for High Throughput Sequence Data. 2010. http://www.bioinformatics.babraham.ac.uk/projects/fastqc/. Accessed Jan 19, 2024.

50. Zheng, G.X.Y., Terry, J.M., Belgrader, P., Ryvkin, P., Bent, Z.W., Wilson, R., Ziraldo, S.B., Wheeler, T.D., McDermott, G.P., Zhu, J., et al. (2017). Massively parallel digital transcriptional profiling of single cells. Nat. Commun. *8*, 14049. https://doi.org/10.1038/ncomms14049.

51. Butler, A., Hoffman, P., Smibert, P., Papalexi, E., and Satija, R. (2018). Integrating single-cell transcriptomic data across different conditions, technologies, and species. Nat. Biotechnol. *36*, 411–420. https://doi.org/10.1038/nbt.4096.

52. Hafemeister, C., and Satija, R. (2019). Normalization and variance stabilization of single-cell RNA-seq data using regularized negative binomial regression. Genome Biol *20*, 296. https://doi.org/10.1186/s13059-019-1874-1.

53. Stuart, T., Butler, A., Hoffman, P., Hafemeister, C., Papalexi, E., Mauck, W.M., 3rd, Stoeckius, M., Smibert, P., and Satija, R. (2019). Comprehensive Integration of Single-Cell Data. Cell *177*, 1888–1902.e21. https://doi.org/10.1016/j.cell.2019.05.031.

54. Korsunsky, I., Millard, N., Fan, J., Slowikowski, K., Zhang, F., Wei, K., Baglaenko, Y., Brenner, M., Loh, P.-R., and Raychaudhuri, S. (2019). Fast, sensitive and accurate integration of single-cell data with Harmony. Nat. Methods *16*, 1289–1296. https://doi.org/10.1038/s41592-019-0619-0.

55. Yu, G., Wang, L.-G., Han, Y., and He, Q.-Y. (2012). clusterProfiler: an R package for comparing biological themes among gene clusters. OMICS *16*, 284–287. https://doi.org/10.1089/omi.2011.0118.

56. Haghverdi, L., Lun, A.T.L., Morgan, M.D., and Marioni, J.C. (2018). Batch effects in single-cell RNA-sequencing data are corrected by matching mutual nearest neighbors. Nat. Biotechnol. *36*, 421–427. https://doi.org/10.1038/nbt.4091.

57. Aibar, S., González-Blas, C.B., Moerman, T., Huynh-Thu, V.A., Imrichova, H., Hulselmans, G., Rambow, F., Marine, J.-C., Geurts, P., Aerts, J., et al. (2017). SCENIC: single-cell regulatory network inference and clustering. Nat. Methods *14*, 1083–1086. https://doi.org/10.1038/nmeth.4463.

58. Love, M.I., Huber, W., and Anders, S. (2014). Moderated estimation of fold change and dispersion for RNA-seq data with DESeq2. Genome Biol. *15*, 550. https://doi.org/10.1186/s13059-014-0550-8.

59. Hänzelmann, S., Castelo, R., and Guinney, J. (2013). GSVA: gene set variation analysis for microarray and RNA-seq data. BMC Bioinformatics *14*, 7. https://doi.org/10.1186/1471-2105-14-7.

60. Korotkevich, G., Sukhov, V., Budin, N., Shpak, B., Artyomov, M.N., and Sergushichev, A. (2016). Fast gene set enrichment analysis. Preprint at bioRxiv. https://doi.org/10.1101/060012.

61. Wickham, H. (2016). ggplot2 - Elegant Graphics for Data Analysis, Second Edition (Springer International Publishing) https://doi.org/10.1007/978-3-319-24277-4.

62. Kolde, R., Laur, S., Adler, P., and Vilo, J. (2012). Robust rank aggregation for gene list integration and meta-analysis. Bioinformatics *28*, 573–580. https://doi.org/10.1093/bioinformatics/btr709.

63. Leek, J.T., Johnson, W.E., Parker, H.S., Jaffe, A.E., and Storey, J.D. (2012). The sva package for removing batch effects and other unwanted variation in high-throughput experiments. Bioinformatics *28*, 882–883. https://doi.org/10.1093/bioinformatics/bts034.

64. Fortin, J., Labbe, A., Lemire, M., Zanke, B.W., Hudson, T.J., Fertig, E.J., Greenwood, C.M., and Hansen, K.D. (2014). Functional normalization of 450k methylation array data improves replication in large cancer studies. Genome Biology *15*, 503. https://doi.org/10.1186/s13059-014-0503-2.

65. Ritchie, M.E., Phipson, B., Wu, D., Hu, Y., Law, C.W., Shi, W., and Smyth, G.K. (2015). limma powers differential expression analyses for RNA-sequencing and microarray studies. Nucleic Acids Res. *43*, e47. https://doi.org/10.1093/nar/gkv007.

66. Van Gassen, S., Callebaut, B., Van Helden, M.J., Lambrecht, B.N., Demeester, P., Dhaene, T., and Saeys, Y. (2015). FlowSOM: Using self-organizing maps for visualization and interpretation of cytometry data. Cytometry A *87*, 636–645. https://doi.org/10.1002/cyto.a.22625.

67. Gu, Z., Eils, R., and Schlesner, M. (2016). Complex heatmaps reveal patterns and correlations in multidimensional genomic data. Bioinformatics. https://doi.org/10.1093/bioinformatics/btw313.

68. Sekhon, J.S. (2011). Multivariate and Propensity Score Matching Software with Automated Balance Optimization: The Matching Package for R. J. Stat. Softw. *42*, 1–52. https://doi.org/10.18637/jss.v042.i07.

69. World Health Organiztion. COVID 19 Therapeutic Trial Synopsis. 2020. https://www.who.int/docs/default-source/blue-print/covid-19-therapeutic-trial-synopsis.pdf. Accessed Jul 23, 2023.

70. Krämer, B., Knoll, R., Bonaguro, L., ToVinh, M., Raabe, J., Astaburuaga-García, R., Schulte-Schrepping, J., Kaiser, K.M., Rieke, G.J., Bischoff, J., et al. (2021). Early IFN-α signatures and persistent dysfunction are distinguishing features of NK cells in severe COVID-19. Immunity *54*, 2650–2669.e14. https://doi.org/10.1016/j.immuni.2021.09.002.

71. Kurth, F., Helbig, E.T., Lippert, L.J., Thibeault, C., Barbone, G., Eckart, M.A., Kluge, M., Puengel, T., Demir, M., Röhle, R., et al. (2023). Cenicriviroc for the treatment of COVID-19: first interim results of a randomised, placebo-controlled, investigator-initiated, double-blind phase II trial. J. Glob. Antimicrob. Resist. *32*, 44–47. https://doi.org/10.1016/j.jgar.2022.12.004.

72. De Domenico, E., Bonaguro, L., Schulte-Schrepping, J., Becker, M., Händler, K., and Schultze, J.L. (2020). Optimized workflow for single-cell transcriptomics on infectious diseases including COVID-19. Star Protoc. *1*, 100233. https://doi.org/10.1016/j.xpro.2020.100233.

73. Hao, Y., Hao, S., Andersen-Nissen, E., Mauck, W.M., Zheng, S., Butler, A., Lee, M.J., Wilk, A.J., Darby, C., Zager, M., et al. (2021). Integrated analysis of multimodal single-cell data. Cell *184*, 3573–3587.e29. https://doi.org/10.1016/j.cell.2021.04.048.

74. Ashburner, M., Ball, C.A., Blake, J.A., Botstein, D., Butler, H., Cherry, J.M., Davis, A.P., Dolinski, K., Dwight, S.S., Eppig, J.T., et al. (2000). Gene Ontology: tool for the unification of biology. The Gene Ontology Consortium. Nat. Genet. *25*, 25–29. https://doi.org/10.1038/75556.

75. The Gene Ontology Consortium (2019). The Gene Ontology Resource: 20 years and still GOing strong. Nucleic Acids Res. *47*, D330–D338. https://doi.org/10.1093/nar/gky1055.

76. Kanehisa, M. (2019). Toward understanding the origin and evolution of cellular organisms. Protein Sci. *28*, 1947–1951. https://doi.org/10.1002/pro.3715.

77. Liberzon, A., Birger, C., Thorvaldsdóttir, H., Ghandi, M., Mesirov, J.P., and Tamayo, P. (2015). The Molecular Signatures Database (MSigDB) hallmark gene set collection. Cell Syst. *1*, 417–425. https://doi.org/10.1016/j.cels.2015.12.004.

78. Fabregat, A., Jupe, S., Matthews, L., Sidiropoulos, K., Gillespie, M., Garapati, P., Haw, R., Jassal, B., Korninger, F., May, B., et al. (2018). The Reactome Pathway Knowledgebase. Nucleic Acids Res. *46*, D649–D655. https://doi.org/10.1093/nar/gkx1132.

79. Gillespie, M., Jassal, B., Stephan, R., Milacic, M., Rothfels, K., Senff-Ribeiro, A., Griss, J., Sevilla, C., Matthews, L., Gong, C., et al. (2022). The reactome pathway knowledgebase 2022. Nucleic Acids Res. *50*, D687–D692. https://doi.org/10.1093/nar/gkab1028.

80. Wu, T., Hu, E., Xu, S., Chen, M., Guo, P., Dai, Z., Feng, T., Zhou, L., Tang, W., Zhan, L., et al. (2021). clusterProfiler 4.0: A universal enrichment tool for interpreting omics data. Innovation (Camb) *2*, 100141. https://doi.org/10.1016/j.xinn.2021.100141.

81. Waltman, L., and van Eck, N.J. (2013). A smart local moving algorithm for large-scale modularity-based community detection. Eur. Phys. J. B *86*, 471. https://doi.org/10.1140/epjb/e2013-40829-0.

82. Subramanian, A., Tamayo, P., Mootha, V.K., Mukherjee, S., Ebert, B.L., Gillette, M.A., Paulovich, A., Pomeroy, S.L., Golub, T.R., Lander, E.S., et al. (2005). Gene set enrichment analysis: a knowledge-based approach for interpreting genome-wide expression profiles. Proc. Natl. Acad. Sci. USA *102*, 15545–15550. https://doi.org/10.1073/pnas.0506580102.

83. Pidsley, R., Zotenko, E., Peters, T.J., Lawrence, M.G., Risbridger, G.P., Molloy, P., Van Djik, S., Muhlhausler, B., Stirzaker, C., and Clark, S.J. (2016). Critical evaluation of the Illumina MethylationEPIC BeadChip microarray for whole-genome DNA methylation profiling. Genome Biol. *17*, 208. https://doi.org/10.1186/s13059-016-1066-1.

84. Ren, X., and Kuan, P.F. (2019). methylGSA: a Bioconductor package and Shiny app for DNA methylation data length bias adjustment in gene set testing. Bioinformatics *35*, 1958–1959. https://doi.org/10.1093/bioinformatics/bty892.

STAR★METHODS

KEY RESOURCES TABLE

REAGENT or RESOURCE	SOURCE	IDENTIFIER
Antibodies		
CD3 BV421 (clone UCHT1)	Biolegend	Cat# 300434; RRID:AB_10962690
CD4 APCFire750 (clone RPA-T4)	Biolegend	Cat# 300560; RRID:AB_2629693
CD8a BV711 (clone RPA-T8)	Biolegend	Cat# 301044; RRID:AB_2562906
CD14 PerCP (clone TÜK4)	Miltenyi	Cat# 130-113-150; RRID:AB_2725978
CD16 BV605 (clone 3G8)	Biolegend	Cat# 302040; RRID:AB_2562990
CD19 PE (clone HIB19)	Biolegend	Cat# 302208; RRID:AB_314238
CD45RA BV785 (clone HI100)	Biolegend	Cat# 304140; RRID:AB_2563816
CD66b APC (clone G10F5)	Biolegend	Cat# 305118; RRID:AB_2566607
CCR7 AF488 (clone G042H7)	Biolegend	Cat# 353206; RRID:AB_10916389
CD45 89Y (Hi30)	Fluidigm	Cat# 3089003; RRID:AB_2938863
CCR2 113In (K036C2)	Biolegend	N/A
CD3 115In (UCHT1)	Biolegend	Cat# 300443; RRID:AB_2562808
CD196 141Pr (G034E3)	Fluidigm	Cat# 3141003A; RRID:AB_2687639
CD49d 141Pr (9F10)	Fluidigm	Cat# 3141004B; RRID:AB_2892684
CD19 142Nd (HIB-19)	Fluidigm	Cat# 3142001B; RRID:AB_2651155
CD123 143Nd (6H6)	Fluidigm	Cat# 3143014B; RRID:AB_2811081
CD15 144Nd (W6D3)	Fluidigm	Cat# 3144019B; RRID:AB_2892685
CD21 145Nd (Bu-15)	Biolegend	Cat# 354902; RRID:AB_11219188
CD138 145Nd (DL101)	Fluidigm	Cat# 3145003B
CD226 146Nd (REA1040)	Miltenyi Biotec	N/A
CD64 146Nd (10.1)	Fluidigm	Cat# 3146006B; RRID:AB_2661790
IgD 147Sm (IgD26)	Biolegend	Cat# 348235; RRID:AB_2563775
CXCR2 147Sm (5E8)	Fluidigm	Cat# 3147010B
ICOS 148Nd (C398.4A)	Fluidigm	Cat# 3148019B; RRID:AB_2756435
CD206 purified (152)	Biolegend	Cat# 321127; RRID:AB_2563729
CD96 purified (REA195)	Miltenyi Biotec	Produced at request
KLRG1 purified (REA261)	Miltenyi Biotec	Produced at request
TCRgd purified (11F2)	Miltenyi Biotec	Produced at request
FceRI 150Nd (AER-37)	Fluidigm	Cat# 3150027B
CD155 purified (REA1081)	Miltenyi Biotec	Produced at request
CD95 purified (DX2)	Biolegend	Cat# 305631; RRID:AB_2563766
CD66b 152Sm (80H3)	Fluidigm	Cat# 3152011B; RRID:AB_2661795
TIGIT 153Eu (MBSA43)	Fluidigm	Cat# 3153019B; RRID:AB_2756419
CD62L purified (DREG56)	Biolegend	Cat# 304835; RRID:AB_2563758
CD1c purified (L161)	Biolegend	Cat# 331502; RRID:AB_1088995
CD27 155Gd (L128)	Fluidigm	Cat# 3155001B; RRID:AB_2687645
CXCR3 156Gd (G025H7)	Fluidigm	Cat# 3156004B; RRID:AB_2687646
CCR5 156Gd (NP-6G4)	Fluidigm	Cat# 3156015A; RRID:AB_2938860
KLRF1 purified (REA845)	Miltenyi Biotec	Produced at request
CD10 158Gd (HI10a)	Fluidigm	Cat# 3158011B; RRID:AB_2921314
CD33 158Gd (WM53)	Fluidigm	Cat# 3158001; RRID:AB_2661799
CD14 160Gd (RMO52)	Fluidigm	Cat# 3160006; RRID:AB_2661801
CD28 purified (L293)	BD Bioscience	Cat# 348040; RRID:AB_400367

(*Continued on next page*)

Continued

REAGENT or RESOURCE	SOURCE	IDENTIFIER
CD69 162Dy (FN50)	Fluidigm	Cat# 3162001B; RRID:AB_3096016
CD294 163Dy (BM16)	Fluidigm	Cat# 3163003B; RRID:AB_2810253
Anti-APC 163Dy	Fluidigm	Cat# 3163001B; RRID:AB_2687636
CXCR5 164Dy (RF8B2)	Fluidigm	Cat# 3164029B
Siglec 8 164Dy (7C9)	Fluidigm	Cat# 3164017B
CD163 165Ho (GHI/61)	Fluidigm	Cat# 3165017B; RRID:AB_2810250
CD34 166Er (581)	Fluidigm	Cat# 3166012B; RRID:AB_2756424
CD38 167Er (HIT2)	Fluidigm	Cat# 3167001B; RRID:AB_2802110
Ki67 168Er (Ki-67)	Fluidigm	Cat# 3168007B; RRID:AB_2800467
CD25 169Tm (2A3)	Fluidigm	Cat# 3169003; RRID:AB_2938861
CD24 169Tm (ML5)	Fluidigm	Cat# 3169004B; RRID:AB_2688021
Lag3 purified (11C3C65)	Biolegend	Cat# 369302; RRID:AB_2616876
RANK purified (80704)	R&D Systems	Cat# MAB683; RRID:AB_2205330
CD161 purified (HP-3G10)	Biolegend	Cat# 339919; RRID:AB_2562836
CD11b purified (ICRF44)	Biolegend	Cat# 301337; RRID:AB_2562811
CD45RO purified (4G11)	DRFZ Berlin	N/A
CD44 purified (BJ18)	Biolegend	Cat# 338811; RRID:AB_2562835
CD137 173Yb (4B4-1)	Fluidigm	Cat# 3173015B
HLA-DR purified (L243)	Biolegend	Cat# 307602; RRID:AB_314680
PD-1 175Lu (EH12.2H7)	Fluidigm	Cat# 3175008; RRID:AB_2687629
PD-L1 175Lu (29.E2A3)	Fluidigm	Cat# 3175017B; RRID:AB_2687638
CD56 176Yb (NCAM16.2)	Fluidigm	Cat# 3176008; RRID:AB_2661813
CD8 purified (GN11)	DRFZ Berlin	N/A
IgM purified (MHM-88)	Biolegend	Cat# 314502; RRID:AB_493003
CD11c purified (Bu15)	Biolegend	Cat# 337221; RRID:AB_2562834
CD16 209Bi (3G8)	Fluidigm	Cat# 3209002B; RRID:AB_2756431
CD14-BV421 (clone M5E2)	Biolegend	Cat# 301830; RRID:AB_10959324
CD163-PercP-Vio700 (clone REA812)	Miltenyi	Cat# 130-112-133; RRID:AB_2655489
CD3-FITC (clone UCHT1)	Biolegend	Cat# 300406; RRID:AB_314060
CD94-FITC (clone DX22)	Biolegend	Cat# 305504; RRID:AB_314534
NKp80-FITC (clone 4A4.D10)	Miltenyi	Cat# 130-094-843; RRID:AB_10829948
TCRab-FITC (clone IP26)	Biolegend	Cat# 306706; RRID:AB_314644
TCRgd-FITC (clone B1)	Biolegend	Cat# 331208; RRID:AB_1575108
CD20-FITC (clone 2H7)	Biolegend	Cat# 302304; RRID:AB_314252
CD19-FITC (clone HIB19)	Biolegend	Cat# 302206; RRID:AB_314236
Amphiregulin-APC (clone AREG559)	Ebioscience	Cat# 17-5370-42; RRID:AB_2716941
Chemicals, peptides, and recombinant proteins		
FcR Blocking Reagent, human	Miletnyi Biotec	Cat# 130-059-901; RRID:AB_2892112
Proteinase K	Sigma-Aldrich	Cat# 3115828001
Tempus™ Blood RNA Tube	ThermoFisher Scientific	Cat# 4342792
PAXgene® Blood RNA Tube	Becton Dickinson	Cat# 762165
SPRIselect	Beckmann Coulter	Cat# B23318
BD Vacutainer® Lithium Heparin Tubes	Becton Dickinson	Cat# 367526
Critical commercial assays		
BD Single-Cell Multiplexing Kit (human)	Becton Dickinson	Cat# 633781
BD Rhapsody WTA Amplification Kit	Becton Dickinson	Cat# 633801
BD Rhapsody Cartridge Kit	BectonDickinson	Cat# 633733

(*Continued on next page*)

Continued

REAGENT or RESOURCE	SOURCE	IDENTIFIER
BD Rhapsody cDNA Kit	BectonDickinson	Cat# 633773
High Sensitivity D5000 ScreenTape	Agilent	Cat# 5067-5592
High Sensitivity D1000 ScreenTape	Agilent	Cat# 5067-5584
Qubit dsDNA HS Assay Kit	ThermoFisher	Cat# Q32851
High Sensitivity DNA Kit	Agilent	Cat# 5067-4626
NovaSeq 6000 S2 Reagent Kit (200 cycles)	Illumina	Cat# 20040326
NovaSeq 6000 S4 Reagent Kit (200 cycles)	Illumina	Cat# 20028313
Chromium Next GEM Single Cell 3′ GEM, Library & Gel Bead Kit v3.1	10x Genomics	Cat# 1000121
Chromium Next GEM Chip G Single Cell Kit	10x Genomics	Cat# 1000120
Single Index Kit T Set A	10x Genomics	Cat# 1000213
TruSeq Stranded Total RNA with Ribo-Zero Globin	Illumina	Cat# 20020613
Maxpar® X8 Antibody Labeling Kit	Fluidigm	Cat# 201146B
Quick-DNA Microprep Kit	Zymo Research	Cat# D3020
EZ DNA Methylation-Gold Kit	Zymo Research	Cat# D5006
Infinium MethylationEPIC BeadChip Kit	Illumina	Cat# WG-317-1002
Zombie Aqua™ Fixable Viability Kit	BioLegend	Cat# 423101
BD Cytofix/Cytoperm™ Fixation/ Permeabilization Kit	Becton, Dickinson	Cat# 554714
SeraSpot Anti-SARS-CoV-2 IgG microarray	Seramun Diagnostica	SP-015-4 G-S12 RUO
Deposited data		
scRNA-seq raw data	This paper	EGAS00001007461, EGAS50000000203
bulk RNA-seq raw data	This paper	EGAS00001007461
processed scRNA-seq count data and code	This paper	https://github.com/knollr/COVID_Dexa
processed bulk RNA-seq count data and code	This paper	https://github.com/knollr/COVID_Dexa
DNA methylation data	This paper	GSE270901
Code for DNA methylation data analysis	This paper	https://github.com/knollr/COVID_Dexa
Software and algorithms		
Bcl2fastq2	Illumina	v2.20
STAR	Dobin et al.[47]	v2.7.3a
Cutadapt	Martin et al.[48]	v1.16
Dropseq-tools	https://github.com/broadinstitute/Drop-seq/	v2.0.0
fastQC	Andrews et al.[49]	0.11.8
10x Genomics Cell Ranger (Software)	Zheng et al.,[50] 10X Genomics	7.0.0
R (bulk and scRNA-seq blood analysis)	https://www.cran.r-project.org	v4.1.0
R (DNA methylation analysis)	https://www.cran.r-project.org	v4.2.1
R (scRNA-seq BAL analysis)	https://www.cran.r-project.org	v4.3.1
Seurat (scRNA-seq blood, R package)	Butler et al.,[51] Hafemeister et al.,[52] Stuart et al.[53]	v4.3.0
Seurat (scRNA-seq BAL, R package)	Butler et al.,[51] Hafemeister et al.,[52] Stuart et al.[53]	v4.4.0
Harmony (R package)	Korsunsky et al.[54]	v0.1.0
ClusterProfiler (R package)	Yu et al.[55]	v4.0.5
batchelor (R package)	Haghverdi et al.[56]	v1.16.0
AUCell (R package)	Aibar et al.[57]	v1.22.0
DESeq2 (R package)	Love et al.[58]	v1.32.0

(*Continued on next page*)

Continued

REAGENT or RESOURCE	SOURCE	IDENTIFIER
GSVA (R package)	Hänzelmann et al.[59]	v1.40.1
fgsea (R package)	Korotkevich et al.[60]	v1.18.0
ggplot2 (R Package; bulk RNA-seq analysis)	Wickham et al.[61]	v3.3.5
ggplot2 (R package; DNA methylation analysis)	Wickham et al.[61]	v3.3.6
pheatmap (R package)	Kolde et al.[62]	v1.0.12
sva (R package)	Leek et al.[63]	v3.44.0
minfi (R package)	Fortin et al.[64]	v1.42.0
limma (R package; DNA methylation analysis)	Ritchie et al.[65]	v3.52.2
limma (R package; bulk RNA-seq analysis)	Ritchie et al.[65]	v3.48.3
methylGSA (R package)	Fortin et al.[64]	v1.14.0
FlowSOM (R package)	Van Gassen et al.[66]	v3.17
uwot (R package)	https://cran.r-project.org/web/packages/uwot/index.html	v0.1.8
ComplexHeatmap (R package)	Gu et al.[67]	v1.20.0
FlowJo	https://www.flowjo.com	v10.8
JMP Pro	SAS Institute inc.	V 16.2.0
Matching (R package)	Sekhon et al.[68]	v4.9-7
OMIQ	www.omiq.ai	N/A

RESOURCE AVAILABILITY

Lead contact

Further information and requests for resources and reagents should be directed to and will be fulfilled by the lead contact, Anna C. Aschenbrenner (anna.aschenbrenner@dzne.de).

Materials availability

This study did not generate new unique reagents.

Data and code availability

scRNA-seq and bulk RNA-seq data generated during this study are deposited at the European Genome-phenome Archive (EGA) under access numbers EGAS00001007461 and EGAS50000000203, which is hosted by the EBI and the CRG. DNA methylation data are deposited on the GEO database under access number GSE270901. All original code has been deposited at GitHub (https://github.com/knollr/COVID_Dexa) and is publicly available as of the date of publication. Any additional information required to reanalyze the data reported in this paper is available from the lead contact upon request.

EXPERIMENTAL MODEL AND STUDY PARTICIPANT DETAILS

Patient cohorts and study flow overview

To determine dexamethasone-specific molecular signatures, samples from patients with dexamethasone treatment and matched controls enrolled into the Pa-COVID-19 study, a prospective, observational study on patients with COVID-19 conducted at Charité Universitätsmedizin Berlin[17] were analyzed using single-cell transcriptomics, CyTOF and flow cytometry. In addition, matched samples from patients with stable versus progressive disease under dexamethasone treatment from the same cohort were assessed for possible influence of the patient's DNA-methylation status on responsiveness to dexamethasone treatment. In a last step, to assess if treatment-related signatures can be used to stratify outcome, bulk-sequencing was performed on samples from patients treated with dexamethasone recruited into the Pa-COVID-19 study and an independent study, PROVID-CAPNETZ, a prospective, observational, multi-centered cohort study with adult SARS-CoV-2 positive hospitalized patients to evaluate clinical data, molecular and functional biomarkers for prognosis, pathomechanisms and treatment strategies of COVID-19 (PROVID) recruited within the competence network community-acquired pneumonia (CAPNETZ, https://capnetz.de). Grouping and selection of patients and a synopsis on clinical characteristics of all included patients and controls per analysis is given in Table S1.

Single-cell transcriptomics, CyTOF, and FACS

In order to determine dexamethasone-specific molecular signatures, all 543 patients included from 1 March 2020 to February 28, 2021 into the Pa-COVID-19 study were screened to identify patients treated with dexamethasone (from June 2020 onwards, following publication of the results of the recovery trial[1]) and comparable patients without dexamethasone treatment (from March to May 2020). Disease severity was stratified using the 8-point WHO ordinal scale[69] of improvement: WHO score 1 and 2 = ambulatory; WHO score 3 = hospitalized without supplemental oxygen; WHO score 4 = hospitalized with low-flow supplemental oxygen; WHO score 5 = hospitalized with requirement of non-invasive ventilation or high-flow oxygen; WHO score 6 = hospitalized with invasive ventilation; WHO score 7 = hospitalized with invasive ventilation and additional organ support; WHO score 8 = death. For analysis WHO grade $\leq$4 was considered as moderate disease, whereas WHO grade $\geq$ 5 was considered as severe disease. WHO score at time point of sampling was used to determine disease severity for these analyses.

Patients meeting one of the following criteria were excluded: age <18 years, no biosamples available, mild disease (maximum WHO score $\leq$3), chronic immunosuppression according to medical history, dexamethasone treatment not following treatment criteria of the recovery trial[1] or any steroid-treatment of control patients recruited early in the pandemic (e.g. hydrocortisone-treatment for septic shock). We also excluded all patients receiving additional immunosuppressive treatments (e.g. TNF-inhibitors, JAK-inhibitors, antimetabolites). This resulted in a total of 153 patients. Sampling timepoints were selected towards the end of the dexamethasone treatment period, and at corresponding time points based on symptom onset for patients without dexamethasone treatment, respectively. To obtain comparable groups (glucocorticoid-naïve controls vs. treated patients), multivariate matching was employed to identify the most suitable matches between groups. Specifically, we used exact matching for treatment with/without dexamethasone, sex, and maximum recorded value of WHO Ordinal Scale during hospitalization and greedy matching with Mahalanobis distance[68] for age and time interval (in days) between symptom onset and acquisition of blood sample closest to the end of dexamethasone treatment. If several equivalent matches were available, patient data was reviewed by two clinically experienced physicians for further details on course of disease (e.g. organ replacement therapy) and pre-existing comorbidities to find the best matches. The most appropriate matches were selected for the respective analyses depending on sample quality (e.g. PBMC count), using the same pairs for scRNASeq, CyTOF, and FACS analysis. If needed for CyTOF and FACS analysis, individual donors were replaced as equivalent as possible and sampling timepoints were adapted to a maximum of +2 days (for CyTOF) and +3 days (for FACS, 1 donor only), respectively.

Subject details blood sc transcriptomics subgroup

A total of 66 PBMC samples from 48 male patients of the Pa-COVID-19 study were selected, with additional 4 samples included from 2 glucocorticoid-naïve patients from an observational study performed at Bonn university hospital fulfilling the same inclusion criteria as described above for the Pa-COVID-19 study.[70]

For analysis of dexamethasone-related signatures, 40 samples collected towards the end of the dexamethasone treatment period of 40 individuals were analyzed. These included 14 treatment-naive (5 moderately ill, 9 severely ill) and 26 dexamethasone-treated patients (7 moderately ill, 19 severely ill). The median age of all patients was 62 years (IQR range 55.25-69.75 years). All moderately affected patients survived, whereas 12 severely ill patients died. Three untreated controls and nine patients treated with dexamethasone. Samples included in analysis of dexamethasone treatment effects were obtained at a median of 8 days (IQR 6.75-9 days) after initiation of dexamethasone treatment and at a median of 15.5 days (IQR 13.75-18 days) after symptom onset. Control samples were obtained at a median of 16 days (IQR 14.75-18 days) after symptom onset.

An additional 26 samples from moderately and severely ill patients were included for comparison and validation of our dataset with previously defined expression changes, but not for analysis of dexamethasone-related signatures. These include samples collected during the early phase of hospitalization of glucocorticoid-naive patients (median 9 days (IQR 7.5-10 days) post symptom onset) and dexamethasone-treated patients (median 6 days (IQR 5-9 days) post symptom onset), as well as early (median 6 days (IQR 5-9 days) post symptom onset) and late (median 13.5 days (IQR 12.25-16.75 days) post symptom onset) samples of patients treated with dexamethasone and the CCR2/CCR5 inhibitor cenicriviroc (CVC[71]), which showed no major effects on single-cell transcriptomes in our analyses.

Subject details FACS subgroup

A total of 36 PBMC samples from 36 male individuals (18 treatment-naive and 18 dexamethasone-treated patients) recruited within Pa-COVID-19 study were analyzed, of which 12 were moderately ill and 24 severely ill. The median age of included patients was 61.5 years (IQR 54-72.25). Samples of dexamethasone-treated patients were obtained at a median of 8 days (IQR 7-10 days) after treatment initiation. Samples were collected at a median of 17 days (IQR 14-18.25 days) after symptom onset for dexamethasone-treated patients vs. 16.5 days (IQR 15-19.25 days) in the untreated control group. Five severely affected patients died, four of whom were in the dexamethasone group and one in the control group.

Subject details CyTOF subgroup

Due to expected decreasing sample quality with storage time and therefore reduced processability, optimization of the sample processing protocol of whole blood samples was applied (see below) and allowed the analysis of limited available samples taken during

the very early pandemic phase before dexamethasone and during the early phase of dexamethasone treatment within this study. Therefore, partial adoption of sampling time points and analyzed individuals was necessary.

A total of 35 samples from 35 patients (1 female, 34 males) recruited within the Pa-COVID-19 study were included into this analysis, 17 of whom were treatment-naive (9 moderately ill, 8 severely ill) and 18 treated with dexamethasone (11 moderately ill, 7 severely ill). The median age of all patients was 61 years (IQR range 54-73 years). All moderately affected patients survived, three severely ill patients deceased, one untreated patient and two patients treated with dexamethasone.

For determination of dexamethasone-related signatures, samples included into analysis were obtained at a median of nine days (IQR 6.75 - 9 days) after initiation of dexamethasone treatment and maximum 24 hours after the last dose. Samples from the dexamethasone-treated group were collected at a median of 15.5 days (IQR 13.75 - 17.25 days) after symptom onset. Control samples were obtained at a median of 15 days (IQR 12.5 - 18 days) after symptom onset.

Subject details BAL sc-transcriptomics subgroup

In order to validate our findings from the blood in lung tissue we furthermore analyzed bronchoalveolar lavages (BAL) obtained from 12 patients recruited in the Pa-COVID-19 study. Due to the limited number of available samples, no matching was performed. In line with the other groups or cohorts, respectively, only immunocompetent glucocorticoid-naive and dexamethasone-treated patients without any additional immunomodulatory COVID-19-specific treatment were included. Samples from dexamethasone-treated patients were included into analysis when collected up to 10 days after the end of treatment. Three patients of the BAL analyses (2 treatment-naive, 1 dexamethasone-treated) were also part of the study population analyzed by blood scRNA-seq.

BALs were obtained during bronchoscopy of invasively ventilated COVID-19 patients at the Department of Infectious Diseases and Respiratory Medicine, Charité Universitätsmedizin Berlin according to standard operating procedures. Among the 12 patients 5 were glucocorticoid-naive (3 males, 2 females), who all survived; 7 received dexamethasone treatment (4 males, 3 females) of whom 4 survived and 3 died. The median age of all patients was 59 years (IQR 33-70 years). BALs were collected at a median of 14 days (IQR 9.5-25 days) after symptom onset from the treatment-naive group and at a median of 23 days (IQR 13-28 days) after symptom onset or 14 days (IQR 8-18 days) after initiation of dexamethasone treatment, respectively, from treated patients.

Epigenetics

To assess the possible influence of patient's DNA-methylation status on responsiveness to dexamethasone treatment, we performed comparative analysis of the included patients from the Pa-COVID-19 study cohort with stable versus progressive disease under treatment, i.e. which progressed from moderate to severe disease or death after having received at least 2 days of treatment with a sample collected within the first 4 days of treatment. Control patients without disease progression under treatment were matched for sex, age, and available early samples after initiation of dexamethasone treatment. If more than one equivalent match was available, data was reviewed by at least two clinically experienced physicians for pre-existing comorbidities to find the most appropriate match.

Subject details epigenetics

A total of 20 samples from 20 dexamethasone-treated patients, 10 males and 10 females, recruited within the Pa-COVID-19 study were analyzed. All 20 patients required supplemental oxygen at treatment initiation without need of invasive mechanical ventilation (WHO score 4-5). The median age of all patients was 62 years (IQR 57.25-69.75 years). Ten out of 20 patients (50%) recovered and did not worsen after initiation of dexamethasone treatment, whereas 10 patients (10/20, 50%) progressed under treatment reflected by the need of invasive ventilation and/or death. Four patients died. Sampling date for analysis was at a median of 2 days (IQR 2-3.75 days) after initiation of dexamethasone and median 9.5 days (IQR 7.25-11.75 days) after symptom onset.

Bulk transcriptomics

To assess if the treatment-related signatures of dexamethasone-treated patients can be used to stratify outcome, bulk-sequencing was performed from the earliest available sample of whole blood collected under dexamethasone treatment from moderately (maximum WHO score $\leq$4) to severely ill (maximum WHO score $\geq$5) COVID-19 patients recruited into two independent cohorts. Patients were grouped according to disease severity as described above. First, patients recruited into the Pa-COVID-19 study in Berlin between 03/2020 and 12/2021 were included into the single-center (Charité) bulk subgroup.

Second, for the independent multi-center (CAPNETZ) cohort, samples were obtained from the CAPNETZ foundation. These patients were recruited across 11 centers (Berlin-Campus Benjamin Franklin, Cottbus, Jena, Bad Arolsen, Dortmund, Bonn, Rotenburg, Dresden, Gerlingen, Berlin-Charité, Berlin-Neukölln) between 06/2020 and 12/2021.

Subject details single-center bulk subgroup

A total of 92 samples from 92 dexamethasone-treated patients (68 males, 24 females) included into the Pa-COVID-19 study were included into this subgroup (single-center, Charité). The median age of all patients was 61 years (IQR 49.75-69 years). Thirty-three patients were moderately ill and 59 patients severely ill, 18 of whom died. Samples for this analysis were obtained at a median 12 days (IQR 9-15 days) after symptom onset and of 4 days (IQR 3-5 days) after the initiation of dexamethasone treatment, respectively.

Subject details multi-center bulk subgroup

A total of 90 samples obtained from 90 dexamethasone-treated patients (65 males, 25 females) included into the multi-center (CAPNETZ) cohort were included into this subgroup. The median age of all patients was 61 years (IQR 52-68 years). A total of 53 patients (65.5%) were moderately ill and 37 (34.4%) were severely ill, 11 of whom (35.5%) died. Samples for this analysis were obtained at a median of 2 days (IQR 1-3) after the initiation of dexamethasone treatment. Symptom onset was not documented in the case reporting form of PROVID-CAPNETZ.

Ethics

The Ethics Committee of Charité Universitätsmedizin Berlin approved the following studies: Pa-COVID-19: EA2/066/20, COV-IMMUN: EA1/068/20. The Ethics Committee of the State Office for Health and Social Affairs Berlin: CVC for COVID-19: 20/0118 – A1 (AMG). The Institutional Review board of the University Hospital Bonn (073/19 and 134/20) approved the study conducted at University Hospital Bonn. The Ethics Committee of Hannover Medical School approved PROVID-CAPNETZ (Nr. 301-2008).

The Pa-COVID-19 study is registered in the German and the WHO international registry for clinical studies (DRKS00021688). The CVC for COVID-19 trial (NCT04500418) and PROVID-CAPNETZ study (NCT04952337) are registered at ClinicalTrials.gov.

The studies were conducted in accordance with the Declaration of Helsinki and current guidelines of Good Clinical Practice. Informed consent was obtained from all participants or their respective legal representatives. All patients were treated according to national and international guidelines.

METHOD DETAILS

Details for blood single-cell transcriptomics

Isolation of blood cells for scRNA-seq

scRNA-seq was performed on frozen PBMCs. Briefly, PBMCs were isolated from heparinized peripheral blood by density centrifugation over Pancoll or Ficoll-Paque density centrifugation (density: 1.077 g/ml). Cells were then cryopreserved at -150°C in RPMI1640 with 40% FBS and 10% DMSO.

BD Rhapsody blood single-cell RNA-seq

Frozen PBMCs were recovered by rapidly thawing frozen cell suspensions in a 37°C water bath followed by immediate serial dilution in pre-warmed RPMI1640+10% FBS (GIBCO) and centrifugation at 300 g for 5 min. After centrifugation, the cells were resuspended in RPMI1640+10% FBS and processed for whole transcriptome analyses, using the BD Rhapsody Single-Cell Analysis System (BD, Biosciences) as previously described[72]. Cells from each sample were labeled with hashtag-oligonucleotide-coupled antibodies, sample tags (BD Human Single-Cell Multiplexing Kit) following the manufacturer's protocol. Briefly, a total number of $1x10^6$ cells were resuspended in 90 μl of Stain Buffer (FBS) (BD PharMingen). The sample tags were added to the respective samples and incubated for 20 min at room temperature. After incubation, 500 μl stain buffer was added to each sample and centrifuged for 5 min at 300 g and 4°C. Samples were washed one more time. Subsequently cells were resuspended in 300 μl of cold BD Sample Buffer and counted using Improved Neubauer Hemocytometer (INCYTO). Labeled samples were pooled equally in 650 μl cold BD Sample Buffer. For each pooled sample two BD Rhapsody cartridges were super-loaded with approximately 60,000 cells each. Single cells were isolated using Single-Cell Capture and cDNA Synthesis with the BD Rhapsody Express Single-Cell Analysis System according to the manufacturer's recommendations (BD Biosciences). cDNA libraries were prepared using the BD Rhapsody Whole Transcriptome Analysis Amplification Kit following the BD Rhapsody System mRNA Whole Transcriptome Analysis (WTA) and Sample Tag Library Preparation Protocol (BD Biosciences). The final libraries were quantified using a Qubit Fluorometer with the Qubit dsDNA HS Kit (ThermoFisher) and the size-distribution was measured using the Agilent high sensitivity D5000 assay on a TapeStation 4200 system (Agilent technologies). Sequencing was performed in paired-end mode (2*75 cycles) on a NovaSeq 6000 with NovaSeq 6000 S2 or S4 Reagent Kit v1.5 (200 cycles) chemistry.

Details for DNA methylation

PBMC isolation for methylation analysis

All samples were obtained in Berlin and subjected to standardized processing and stored by the Central Biobank of Charité (ZeBanC) according to SOPs of the Pa-COVID-19 study.

FACS-based cell isolation for methylation analysis

Frozen PBMC samples were taken up in 37°C RPMI1640 medium (Gibco) containing 20% BSA Fraction V (PAN-Biotech), 1% 10,000 U/ml Penicillin Streptomycin (Thermo Fisher Scientific) and 10 mM Hepes buffer (Biochrom) to quickly thaw. Cells were washed with PBS (Gibco).

PBMCs were stained using the following fluorescently conjugated monoclonal antibodies: CD3 BV421 (clone UCHT1), CD4 APCFire750 (clone RPA-T4), CD8a BV711 (clone RPA-T8), CD14 PerCP (clone TÜK4), CD16 BV605 (clone 3G8), CD19 PE (clone HIB19), CD45RA (clone HI100), CD66b APC (clone G10F5), CCR7 AF488 (clone G042H7).

$CD14^+$ Monocytes ($CD14^+$, $CD16^-$, $CD66b^-$), $CD19^+$ B cells ($CD3^-$, $CD19^+$), $CD4^+$ total memory T cells ($CD3^+$, $CD4^+$, $CD45RA^-$ and $CD3^+$, $CD4^+$, $CD45RA^+$, $CCR7^-$) and $CD8^+$ total memory T cells ($CD3^+$, $CD8^+$, $CD45RA^-$ and $CD3^+$, $CD8^+$, $CD45RA^+$, $CCR7^-$) were

sorted via FACS with a BD FACSAria II SORP (Becton Dickinson). Checks for sort purity were performed and ranged between 90%–99%. Following FACS, cell pellets were flash-frozen in liquid nitrogen.

DNA methylation profiling

From purified cell samples frozen as pellets, genomic DNA was extracted using Zymo's Quick-DNA MicroPREP Kit (Zymo Research) following instructions provided by the manufacturer. DNA concentration was measured using the Qubit dsDNA HS Assay Kit and the Qubit Fluorometer (Molecular Probes/Life Technologies).

Samples with cell counts <25,000 cells were not subjected to DNA extraction. Instead, the cell pellets were directly taken up in a mix of 40 μl lysate buffer from the Zymo's Quick-DNA MicroPREP Kit (Zymo Research) with 1.25 mg/ml Proteinase K (Sigma-Aldrich 3115828001) and incubated for 3 hours at room temperature. Cell lysate was directly used for bisulfite conversion as described below.

Isolated genomic DNA and cell lysates from Proteinase K digestion were subjected to bisulfite conversion using Zymo's EZ DNA Methylation-Gold Kit (Zymo Research) according to manufacturer's instructions. DNA methylation was assessed using the Infinium MethylationEPIC Kit (Illumina EPIC-8 BeadChip) following manufacturer's instructions. Illumina EPIC-8 BeadChips were imaged using Illumina's Microarray Scanner iScan.

Details for CyTOF

Antibodies used for CyTOF

All anti-human antibodies pre-conjugated to metal isotopes were obtained from Fluidigm Corporation (San Francisco, USA). All remaining antibodies were obtained from the indicated companies as purified antibodies and in-house conjugation was done using the MaxPar X8 labeling kit (Fluidigm, USA). Antibodies are listed in the key resource table.

Sample processing and antigen staining for CyTOF

Sample processing, cell staining and acquisition was done as previously described.[18] In brief, whole blood samples were thawed, tagged with barcoding antibodies conjugated with different isotopes of Pd or Pt for 30min at 4°C and up to 10 samples were pooled for surface and intracellular staining. For surface staining, samples were incubated with primary and secondary anti-APC163Dy antibodies for 30min at 4°C, respectively, washed with PBS and fixed overnight. For intracellular staining, samples were permeabilized with permeabilization buffer (eBiosciecne, San Diego, US), stained with the respective antibodies for 30min at room temperature, and washed and stained with iridium intercalator (Fluidigm) for 20min at room temperature. After staining, cells were washed and stored at 4°C. Mass cytometry measurement was performed on a CyTOF2/Helios mass cytometer (Fluidigm).

Details for bulk transcriptomics

Whole blood RNA isolation

For the single-center (Charité Berlin) and multi-center cohort (CAPNETZ), whole blood RNA isolation strategies were applied. In cohort 1, whole blood was collected and stored in Tempus tubes (Applied Biosystems), while cohort 2 used the PAXgene system (BD Medical). RNA was extracted according to the manufacturer's information.

Bulk RNA sequencing

After RNA extraction, total RNA libraries were generated using the TruSeq Stranded Total RNA with Ribo-Zero Globin kit (Illumina). In brief, ribosomal and globin mRNA were depleted from 750 ng purified total RNA using biotinylated, target-specific oligos combined with Ribo-Zero rRNA removal beads; after depletion remaining RNA was purified, fragmented, and primed for cDNA synthesis. 3′ ends were adenylated and index adapters were ligated to the ends of the ds cDNA. Selective enrichment of DNA fragments with ligated adaptor molecules on both ends was performed using Illumina PCR primers in a 15-cycle PCR reaction, followed by a purification step using SPRIBeads (Beckman Coulter). Libraries were quantified by Qubit dsDNA HS Assay (Thermo Fisher Scientific), and fragment size distribution was determined using the HS D1000 assay on a Tapestation 4200 system (Agilent). Sequencing was performed in paired-end mode (2*50 cycles) on a NovaSeq 6000 with NovaSeq 6000 S2 Reagent Kit v 1.5 (200 cycles) chemistry. Data was converted into fastq files using bcl2fastq2 v2.20.

BAL single-cell processing and sequencing

BALs were processed and sequenced as described before.[30] BAL fluid was filtered through a 70 μm mesh and centrifuged (400 g, 10 min, 4°C). The supernatant was removed and cells were washed once with DPBS (GIBCO). Erythrocytes were then removed using the Red Blood Cell (RBC) lysis buffer (Biolegend). The cells were washed twice and either processed for subsequent scRNA-seq or cryopreserved in FCS+10% DMSO at -150°C.

Frozen BAL cells were thawed using pre-warmed medium (RPMI 1640, Gibco; 2% FCS, Sigma; 0.01% Pierce Universal Nuclease, Thermo Fisher, USA). For multiplexing of multiple BAL donors, cells were labeled with 0.5μg of TotalSeq-A Hashtag antibodies for 30 min at 4°C. Subsequently cells were washed three times and up to 4 donors were pooled in equal proportions and passed through a 40 μm mesh (Flowmi™ Cell Strainer, Merck).

The cell suspension was then adjusted to an appropriate concentration to load 16.500- 50.000 cells/reaction into the 10x Genomics Chromium Controller for scRNA-seq. Single Cell 3′ reagent kit v3.1 was used for reverse transcription, cDNA amplification and library construction according to the detailed protocol provided by 10x Genomics and Biolegend. Libraries were quantified by QubitTM 2.0 Fluorometer (ThermoFisher) and quality was checked using 2100 Bioanalyzer or Tapestation 4150 with High Sensitivity

DNA kit (Agilent). Sequencing was performed in paired-end mode with SP, S1, S2 (2x50 cycles) and S4 (2x100 cycles) flowcells using NovaSeq 6000 sequencer (Illumina).

Monocyte FACS verification

CD163 and amphiregulin expression in monocytes was assessed by flow cytometry. Briefly, after treatment with Zombie Aqua viability dye (Biolegend, USA), FC receptor blockade (FC Block, Miltenyi), thawed PBMCs were incubated with following surface antibodies: CD14-BV421 (clone M5E2), CD163-PercP-Vio770 (clone REA812), and for exclusion CD3-FITC (clone UCGT1), CD94-FITC (clone DX22), NKp80-FITC (clone 4A4.D10), TCRab-FITC (clone IP26), TCRgd-FITC (clone B1), CD20-FITC (clone 2H7), and CD19-FITC (clone HIB19). Samples were analyzed using a BD Canto II flow cytometer and FlowJo 10.8 software (BD).

SARS-CoV-2 spike protein ELISA

SARS-CoV-2 spike protein-specific antibodies were detected by SeraSpot Anti-SARS-CoV-2 IgG microarray-based multiparameter immunoassay. Samples were processed and measured according to the manufacturer's instructions (Seramun Diagnostica GmbH, https://www.seramun.com). In brief, serum samples were pre-diluted 1:101 and added to microarray plates pre-coated with the SARS-COV-2 receptor-binding domain (RBD) epitope, with negative and positive controls as capture antibodies. Samples were measured with the accompanying SpotSight plate scanner and results above 160 BAU/ml were regarded as positive, as per the manufacturer.

QUANTIFICATION AND STATISTICAL ANALYSIS

Analysis of blood single-cell transcriptome data

Data pre-processing of blood scRNA-seq data

After demultiplexing of bcl files using Bcl2fastq2 V2.20 from Illumina and quality control, paired-end scRNA-seq reads were filtered for valid cell barcodes using the barcode whitelist provided by BD. Cutadapt 1.16 was then used to trim NexteraPE-PE adaptor sequences where needed and to filter reads for a PHRED score of 20 or above.[48] Then, STAR 2.7.3a was used for alignment against the Gencode v27 reference genome.[47] Dropseq-tools 2.0.0 were used to quantify gene expression and collapse to UMI count data (https://github.com/broadinstitute/Drop-seq/). For hashtag-oligo based demultiplexing of single-cell transcriptomes and subsequent assignment of cell barcodes to their sample of origin the respective multiplexing tag sequences were added to the reference genome and quantified as well.

Blood scRNA-seq quality control and annotation

Samples were selected and grouped as described above. Analysis of scRNA-seq data was performed using the Seurat pipeline (v4.3.0).[51,73] During preprocessing and quality control (QC), cells that were considered as doublets or negatives after demultiplexing using the HTODemux function from Seurat (positive.quantile 0.99), singlets that did not exceed 300 unique molecular identifiers (UMIs), had more than 30% mitochondrial genes, showed less than 300 and more than 3500 features per cell or were present in small contaminating clusters were excluded from downstream analysis. Additionally, genes that were expressed in less than 5 cells per cartridge were removed. After QC, a total of 114,181 single-cell transcriptomes of PBMCs were analyzed. The entire dataset was normalized, scaled, and dimensional reduction was calculated using the standard Seurat functions. For normalization, the gene expression values were normalized by total UMI counts per cell, multiplied by 10,000 (TP10K) and then log transformed by $\log_{10}$(TP10k+1). Subsequently, the data was scaled, centered, and regressed against the number of detected transcripts per cell to correct for heterogeneity associated with differences in sequencing depth. For dimensionality reduction, PCA was performed on the top 2,000 variable genes identified using the vst method. For two-dimensional representation of the data structure, uniform manifold approximation and projection (UMAP) was calculated using the first 30 principle components (PCs). Subsequently, the cells were clustered using the Louvain algorithm based on the first 30 PCs using a resolution of 0.4. Cluster-specific marker genes were calculated with the Wilcoxon rank sum test using the FindAllMakers function (min.pct=0.2, logfc.threshold=0.5). Using the combined information of cluster marker and literature-known markers, present cell types were annotated: Monocytes (*LYZ, S100A8, S100A9*), mDCs (*FCER1A, CD1C*), pDCs (*ITM2C, SOX4*), platelets (*PPBP, PF4*), $CD4^+$ T cells (*TCF7, IL7R*), $CD8^+$ T cells (*CD8A, GZMH*), NK cells (*KLRF1, PRF1*), B cells (*MS4A1, CD79A*), plasmablasts (*JCHAIN, IGKC*), proliferating cells (*MKI67, STMN1*) and erythrocytes (*HBB, HBA1, HBA2*).

Selection of monocytes

Blood monocytes were selected and annotated in a three-step process. First, all monocyte transcriptomes were subsetted from the PBMC data. This subset was subsequently normalized and scaled, and dimensional reduction was calculated using the standard Seurat functions. For normalization, the gene expression values were normalized by total UMI counts per cell, multiplied by 10,000 (TP10K) and then log transformed by $\log_{10}$(TP10k+1). Subsequently, the data was scaled, centered, and regressed against the number of detected transcripts per cell to correct for heterogeneity associated with differences in sequencing depth. For dimensionality reduction, PCA was performed on the top 1000 variable genes identified using the vst method. To adjust for a batch-effect observed by experimental day, the harmony algorithm (v0.1.0) was applied.[54] For two-dimensional representation of the data structure, uniform manifold approximation and projection (UMAP) was calculated using the first 15 harmony components. Next, monocytes were cleaned from non-monocytes. For this, the cells were clustered using the Louvain algorithm based on the first 15 harmony

reductions. Clusters showing expression of other cell types (such as NK cells, T cells and B cells) were excluded. Finally, after cleaning, the basic Seurat steps were applied again and clusters were calculated using a resolution of 0.7. Cluster-specific marker genes were calculated with the Wilcoxon rank sum test using the FindAllMakers function (min.pct=0.2, logfc.threshold=0.5). The resulting monocyte clusters were annotated as IFI^{hi} (*IFI6, IFI27, IFI44L*), IL1B^{hi} (*IL1B, CCL3, CCL4L2*), S100A^{hi} (*S100A12, S100A8, S100A9*), S100A^{hi}CXCL^{hi} (*CXCL1, CXCL2, CXCL3, CXCL8*), Dexa response (*AREG, IL1R2, CD163, TSC22D3*), HLA^{hi} (*HLA-DPA1, HLA-DRA, HLA-DRB1*), THBD^{hi} (*THBD, RGCC, LMNS*), PF4^{+} (*PF4*), HB^{hi} (*HBB*) and CD16 C1Q^{+} (*FCGR3A, C1QB, C1QA*) monocytes.

Module score calculation

For the module score calculation, the AddModuleScore function from Seurat was applied with the respective gene signatures.

For the interferon enrichment a set of 15 interferon-response genes was used including *IFI6, ISG15, IFITM1, ISG20, IFI27, IFI30, IFIH1, IFIT1, IFIT2, IFIT3, IFITM2, IFITM3, XAF1, MX1* and *MX2*. For the glucocorticoid signature the top 100 up- and downregulated genes from Wang et al.[26] were extracted and enriched by blood monocyte states.

To check for statistical differences, a Kruskal-Wallis (KW) test was applied for the mean module score per donor against the respective category of interest, e.g. monocyte states.

Differential gene expression

Differential expression (DE) tests in the blood data were performed using FindMarkers function from Seurat with the Wilcoxon rank sum test. Genes with a log-fold change greater than 0.25, at least 10% expressed in tested groups and with a bonferroni-corrected p value ≤ 0.05 were considered as significantly differentially expressed genes (DEGs). For calculation of DEGs by cell types, only cell types with more than 2,000 cells were considered.

Functional enrichment analysis

Gene set ontology enrichment analysis (GOEA) using the DEGs as input was performed on the gene sets from the Gene Ontology (GO) biological process (BP) database,[74,75] the Kyoto Encyclopedia of Genes And Genomes (KEGG) database,[76] the Hallmark gene sets[77] and the Reactome gene sets[78,79] using the R package clusterProfiler (version 4.0.5).[55,80] Ontologies with statistical significance (bonferroni-adjusted p value ≤ 0.05) were used for presentation. For the common terms in multiple cell types, terms were filtered for enrichment in at least three different cell types.

Quantification of monocyte states

To compare shifts in the blood monocyte states stratified by group and treatment as well as outcome, the percentages of each cluster were quantified per sample of the respective groups and visualized together in boxplots. For determination of statistical significant differences in the distribution a Wilcox test was performed for severity or outcome groups.

Core Dexa signature identification

To identify DEGs common for Dexa treatment despite COVID-19 severity, a fold change (FC) comparison was performed for DEGs calculated between Dexa vs. ctrl. for both severities independently. Resulting FCs were plotted against each other and commonly up- and downregulated genes were indicated.

Analysis of BAL single-cell transcriptome data

Re-analysis of BAL monocytes from Sinha et al.

To verify our findings from our scRNA-seq monocyte analysis, we inspected the single-cell whole blood dataset generated by Sinha et al.[12] The monocyte compartment was subsetted based on the original 'celltype1' annotation. Subsequently, the monocytes were normalized, scaled, and visualized using 'patient'-corrected harmony and UMAP dimensionality reductions. After removal of contaminating clusters, defined as cells that express cell type markers unrelated to monocytes, a total of 2,350 monocytes were present. By *CD14* and *FCGR3A* (CD16) expression, the monocytes were annotated as classical or non-classical monocytes. In all monocytes, the average expression of selected Dexa-related genes was calculated stratified by the "time_split_status" information provided by the authors (including treatment group and duration) and visualized in a heatmap.

Re-analysis of BAL myeloid cells from Liao et al.

To check specific genes identified in this study in the lung, we inspected the single-cell bronchoalveolar lavage (BAL) dataset generated by Liao et al.[29] Here, a total of 6 severe COVID-19 patients were included with n=2 untreated survivors and n=4 methylprednisolone-treated patients, of which n=2 deceased. The macrophage and monocyte compartment was subsetted based on the original cell type annotation, cells were cleaned from contamination and gene expression of 32 selected markers was assessed in a total of 25,191 cells.

BAL scRNA-seq pre-processing, quality control, and annotation

Raw expression data in form of FASTQ files were collected, read quality was assessed using fastQC (version 0.11.8)[49] and alignment/counting was performed using 10x Genomics Cell Ranger (version 7.0.0)[50] using a custom reference created from the GRCh38 human genome reference available from 10x Genomics (refdata-gex-GRCh38-2020-A) and a number of viral genomes including SARS-CoV-2 (RefSeq:NC_045512.2).

For quality control, transcriptomes were clustered using library size, number of genes, percentage of mitochondrial (%MT) and ribosomal (%RP) counts. Clusters with %MT > 5 were excluded from the analysis. After QC, a total of 67,439 single-cell transcriptomes of BAL cells remained.

Data was loaded into R (version 4.3.1) and stored in a SeuratObject (version 4.1.4). Seurat (version 4.4.0)[51,73] was used to normalize counts, find variable genes, scale data, and compute a PCA embedding. FastMNN from the batchelor package (version 1.16.0)[56] was used to integrate data using ''library'' as a batch. For annotation, clusters were computed using the Seurat implementation of the smart local moving algorithm for large-scale modularity-based community detection,[81] cell type AUCs were computed using the AUCell package (version 1.22.0)[57] and automatic assignment of cell type identity to clusters was performed using annotate_maxAUC of the SeuratHelper package (version 1.0.0). Annotation was refined using cluster averages of AUC scores and quality metrics. Cell types annotation markers: Monocytes (*CD14, VCAN, FCGR3A*), macrophages (*MARCO, CD68*), DCs (*TCF4, CD1C*), T cells (*CD8A, CD3D, CD3E*), plasmablasts (*JCHAIN, IGHGP*), neutrophils (*CSF3R, NAMPT*), erythrocytes (*HBA1, HBB*) and epithelia (*KRT8, KRT19*).

Custom code used for the analysis is available under github.com/saliba-lab/covid19-bal-atlas-integration.

Differential gene expression

Differential expression (DE) tests in the BAL data were performed using FindMarkers function from Seurat with the Wilcoxon rank sum test. Genes with a log-fold change greater than 0.25, at least 10% expressed in tested groups and with a bonferroni-corrected p value ≤ 0.05 were considered as significantly differentially expressed genes (DEGs). For calculation of DEGs by cell types, erythrocytes and low-quality cells were excluded.

Module score calculation

For the module score calculation in BAL monocytes and macrophages, the AddModuleScore function from Seurat was applied with the ''Dexa response'' monocyte state markers (n=30) as a signature. For statistical testing, a Wilcoxon test was performed based on the mean module score per donor by the respective treatment groups and outcome.

Bulk RNA-sequencing analysis

The 'STAR: ultrafast universal RNA-seq aligner' (v2.7.3a)[47] was used to align the sequenced reads against the human GENCODE reference genome v33. Total reads were randomly downsampled to a maximum of 34,195,155 reads per sample. Following the import of the raw counts using the DESeq2[58] function DESeqDataSetFromMatrix, genes with a lower total count number than the included number of samples were excluded from the analysis resulting in 27,669 and 28,784 genes for cohort 1 and cohort 2, respectively. The count matrices were DESeq2 normalized and a variance stabilizing transformation (vst) was applied. To minimize the variance introduced by the different study sites in cohort 2, the transformed data was limma batch-corrected[65] setting the study sites and the seasonality as the batch variables. Patient groups were defined as described above. A gene set variation analysis (GSVA)[59] was performed on the transformed data with default parameters using the single-cell RNA-seq monocyte outcome signature, which was based on the comparison of dexamethasone-treated but deceased patients vs. treated survivors ('deceased upregulated' with 379 genes and 'deceased downregulated' with 282 genes). Wilcoxon tests were calculated between the different conditions and the resulting p values were adjusted utilizing the Benjamini-Hochberg (BH) method. Permutation tests were performed by drawing 500 random, unique gene sets with the same size as the respective signature. For each gene set, GSVA enrichment scores were calculated per sample and BH-adjusted p values were computed between surviving and deceased patients. The likelihood of the enrichment results of the single-cell signatures was computed by dividing the number of gene sets with lower adjusted p values by the number of permutations. To identify the optimal signature length, signature genes measured in both cohorts (366 genes in the 'deceased upregulated'-signature and 275 genes in the 'deceased downregulated'-signature) were ordered based on their average log2FC in the scRNA-seq data and a GSVA was performed for all possible signature sizes in each cohort (starting with an initial size of 10 signature genes). The optimal signature length was defined as the minimum of the mean adjusted p value distribution of the two cohorts. Genes representing the leading edge of each signature enrichment were assessed by calculating the expression level statistics from a non-parametric kernel estimation of the cumulative density function of each gene expression profile per sample and cohort as previously described.[59] After computing the mean of the expression level statistic for each gene over all samples of the deceased patient group of the respective cohort and centering the resulting ranks around 0, a gene set enrichment analysis (GSEA) was performed per signature and cohort and the leading edge defined as the subset of the signature including those genes that appear in the ranked list at or before the point at which the running sum reaches its maximum[82] was computed using fgsea (v1.18.0).[60]

CyTOF: Cell identification and cluster analysis

Major leukocyte populations were identified from two antibody panels designed for CyTOF. Myeloid cells were identified from panel 2. Monocytes and DCs were obtained from the exclusion of $CD3^-$, $CD19^-$ and $CD56^-$ cells, and expression of $CD14^+$ and $HLA\text{-}DR^+$ cells. The Monocytes and DCs batch-normalized CyTOF values (described in Schulte-Schrepping et al.[18]) were first transformed with the inverse hyperbolic sine function (asinh) and then z-score normalized per marker across all samples and all cells. They were then clustered using FlowSOM,[66] with 25 meta clusters (FlowSOM_k). Clusters were merged in pairs when their marker expressions were similar, which resulted in 19 clusters (Figure S3B). Similarly, UMAPs were calculated with the selected markers mentioned above using the R package 'uwot' with default parameters (https://github.com/jlmelville/uwot). The frequency of each cluster was calculated as the percentage of cells in each cluster for each sample in each compartment.

Statistical testing for the difference in the frequency of each cluster per severe or moderate category was calculated with the Wilcoxon test. Granulocytes in panel 2 were identified based on the expression or exclusion of $CD3^{-}CD19^{-}CD56^{-}CD14^{-}CD15^{+}$. Populations obtained from panel 1 include:

$CD4^{+}$ T cells ($CD3^{+}CD45^{+}CD19^{-}CD15^{+}CD14^{+}CD8^{-}TCRgd^{-}$), $CD8^{+}$ T cells ($CD3^{+}CD45^{+}CD19^{-}CD15^{+}CD14^{+}CD8^{-}TCRgd^{-}$) and $TCRgd^{+}$ cells ($CD3^{+}CD45^{+}CD19^{-}CD15^{+}CD14^{+}TCRgd^{+}$). Other populations include the B cells ($CD45^{+}CD19^{+}CD3^{-}CD14^{-}CD15^{-}$) and NK cells ($CD45^{+}CD3^{-}CD19^{-}CD56^{+}CD14^{-}$).

Analysis of DNA methylation data

Pre-processing raw methylation data

The raw intensity data files (IDAT) were preprocessed using minfi version 1.42.0 by quantile normalization. Probes were filtered based on not meeting the detection *p* value threshold against the background ($p<0.01$), being reported as cross-reactive,[83] revisions of Illumina's manifest (Infinium MethylationEPIC v1.0 13.03.2020), or being at a SNP, using the minfi function dropLociWithSnps. To account for differences between the 10 matched responder/non-responder pairs (e.g. matched comorbidities, age, sex, etc.) batch correction was performed using the ComBat function from the sva package version 3.44.0.[63]

Differential DNA methylation analysis

As the cohort included both female and male donors, CpGs on sex chromosomes were removed before differential methylation analysis. Differential methylated positions (DMPs) were identified using the limma package version 3.52.2.[65]

Enrichment analysis for DNA methylation data

Gene set ontology enrichment analysis adjusting for CpG number per gene using DMPs as input was performed using the methylglm function from the mehylGSA package version 1.14.0[84] on gene sets from the Gene Ontology (GO) biological process (BP) database.[75]

Enrichment of differentially expressed genes from the scRNA-seq dataset was calculated using the methylRRA function from the same package. The function utilizes robust rank aggregation (RRA) to adjust multiple *p* values of each gene for enrichment analysis.[62]

Data visualization

For data visualization the R packages Seurat (version 4.3.0),[73] ggplot2 (version 3.3.5),[61] pheatmap (version 1.0.12) or fmsb (version 0.7.5) were used.

CellPress
OPEN ACCESS

Supplemental figures

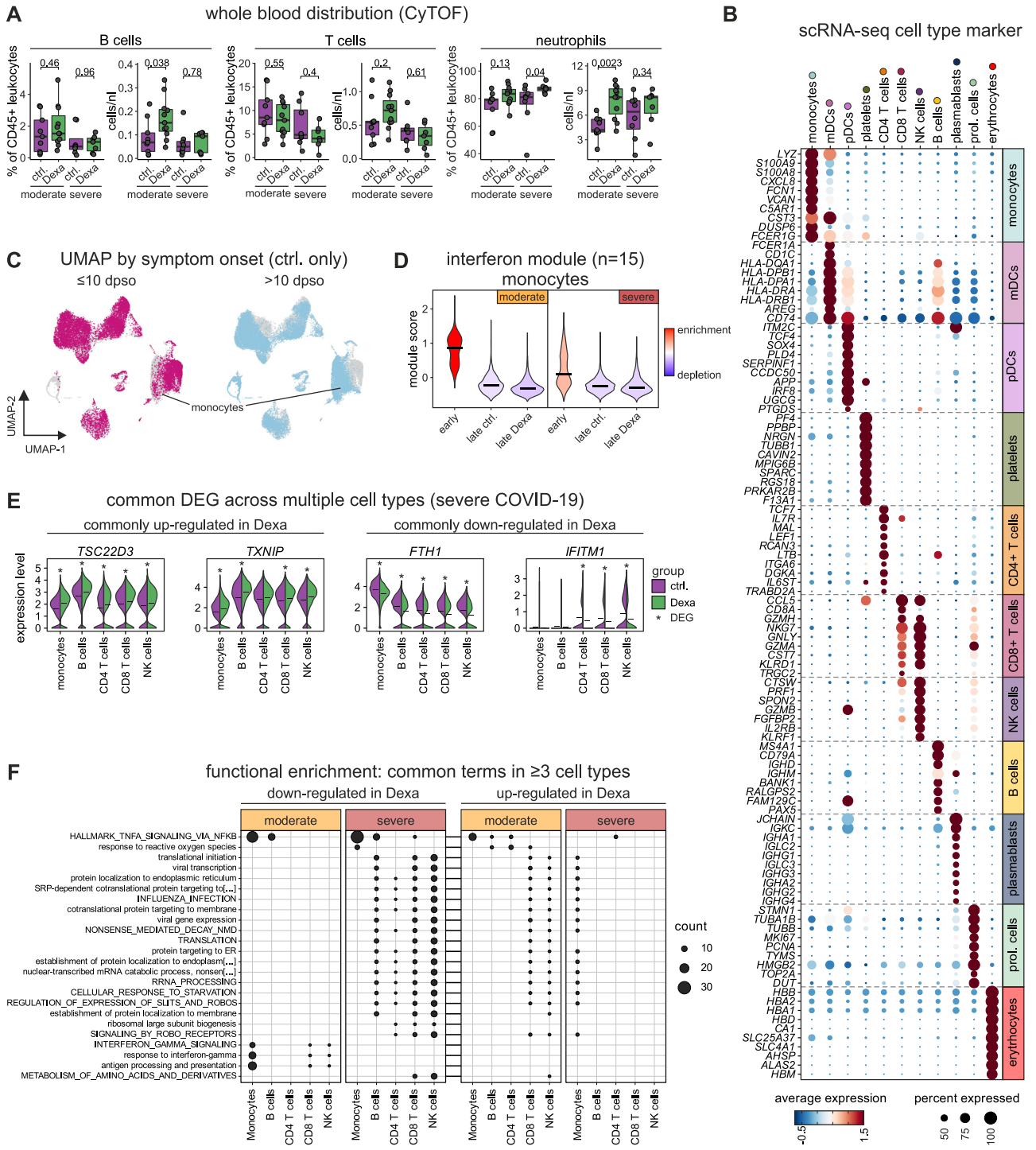

Figure S1. Shared effect of dexamethasone treatment across circulating immune cells, related to Figure 1

(A) Percentages of CD45^{+} leukocytes and concentration of B cells, T cells, and neutrophils in whole blood from CyTOF stratified by treatment and COVID-19 severity. Wilcoxon test for statistical significance, and resulting *p* values are indicated.

(B) Marker gene expression for identified major cell types in the PBMC space from single-cell RNA-seq data.

(legend continued on next page)

(C) UMAP of the entire PBMC space from scRNA-seq colored by symptom onset in days after onset ($\leq$10 or >10) for untreated patients (control).
(D) Enrichment of the interferon module (n = 15 genes) described for acute COVID-19 monocytes[18] in monocytes by time points.
(E) Common differentially expressed genes (DEGs, from Figure 1G) in at least 3 cell types in severe COVID-19. Significant differential expression is indicated with asterisks.
(F) Functional enrichment of DEGs identified in Figure 1G using the GO biological processes (BP) and Hallmark databases. Displayed terms were common in at least three cell types.

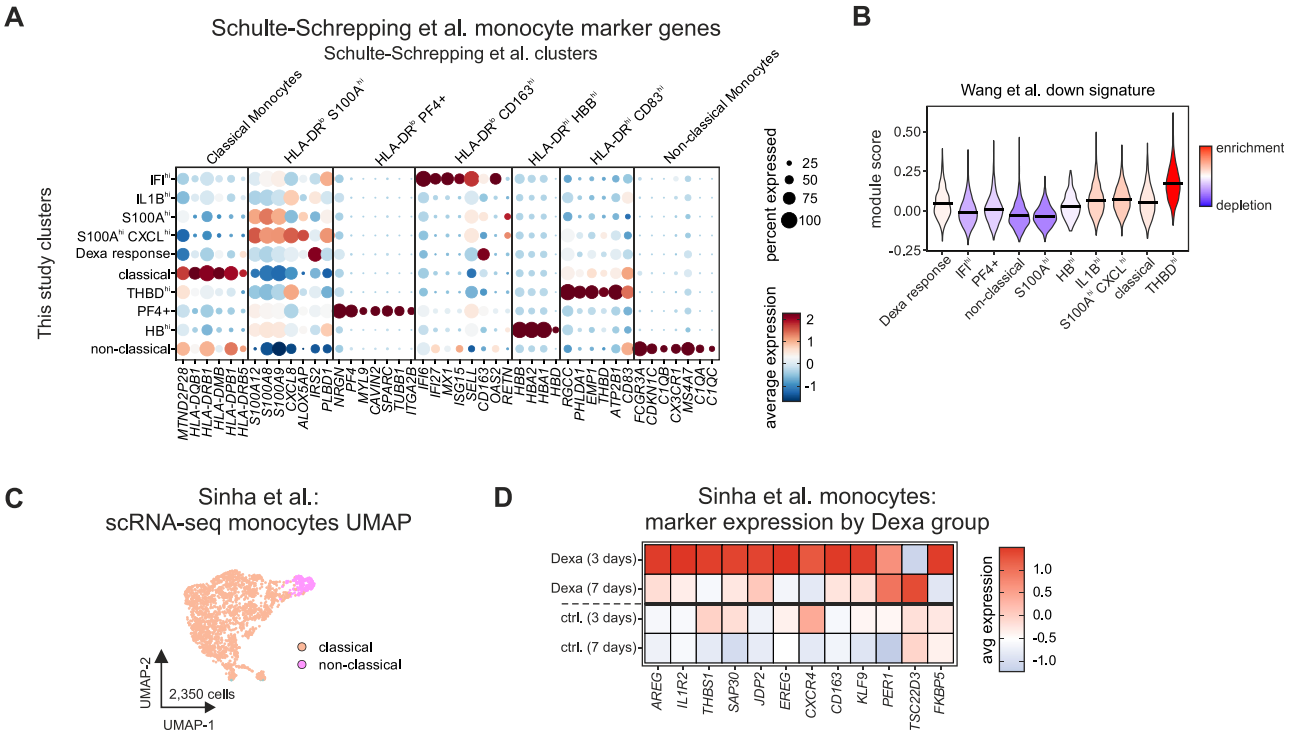

Figure S2. Mapping of monocyte states to acute COVID-19 and validation of dexamethasone effects, related to Figure 2

(A) Expression of monocyte-state markers from Schulte-Schrepping et al.[18] by monocyte states identified in this study.

(B) Enrichment of the *in vitro* generated glucocorticoid down signatures from Wang et al.[26] in all monocyte states.

(C) UMAP visualization of all monocytes extracted from the whole blood scRNA-seq dataset from Sinha et al. (n = 2,350 cells).[12]

(D) Dexa-inducible gene expression in whole blood monocytes of dexamethasone-treated and control patients separated for time points (3 and 7 days) from Sinha et al.[12]

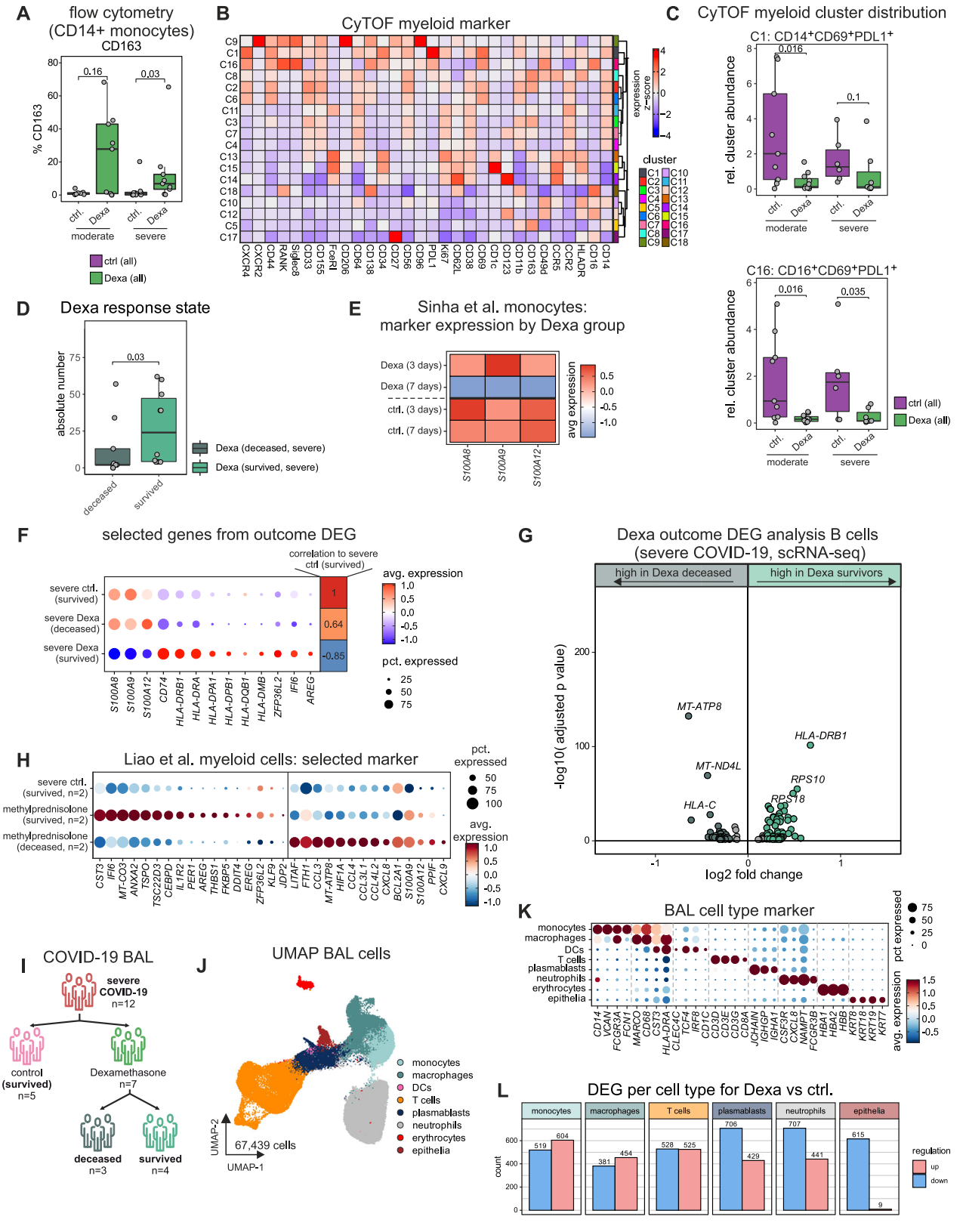

(legend on next page)

Figure S3. Proteomics analysis of monocytes and overview of the BAL dexamethasone cohort, related to Figure 3

(A) CD163 protein expression by flow cytometry on $CD14^+$ monocytes of COVID-19 patients who survived stratified by severity and dexamethasone treatment. Wilcoxon test for statistical testing, and resulting *p* values are indicated.

(B) Clustered marker heatmap of the CyTOF analysis from myeloid cells with a total of 18 clusters defined by 31 protein markers. Resulting clusters are indicated.

(C) Monocyte relative cluster distribution from CyTOF analysis for clusters 1 ($CD14^+CD69^+PD\text{-}L1^+$) and 16 ($CD16^+CD69^+PD\text{-}L1^+$) in COVID-19 patients who survived stratified by severity and dexamethasone treatment. Wilcoxon test for statistical testing, and resulting *p* values are indicated.

(D) Absolute numbers of monocyte in the Dexa response state in severe patients with dexamethasone treatment stratified by outcome. Statistical testing using Wilcoxon test, and resulting *p* values are indicated.

(E) Alarmin (*S100A8*, *S100A9*, and *S100A12*) gene expression in whole blood monocytes selected from Sinha et al. (see Figure S2C).[12]

(F) Gene expression of selected genes from the monocyte outcome signature (Figure 3H) by COVID-19 severity status and outcome in monocytes. Correlation of the average gene expression of those genes compared with severe controls that survived is indicated.

(G) Volcano plot showing the outcome DEGs between severe COVID-19 patients treated with dexamethasone who survived vs. those who were treated but deceased in B cells.

(H) Expression of selected markers identified in this study in the bronchoalveolar lavage (BAL) COVID-19 macrophages and monocytes from Liao et al.[29] comprising $n = 6$ severe COVID-19 patients with $n = 2$ untreated survivors and $n = 4$ methylprednisolone-treated patients of which 2 deceased.

(I) COVID-19 BAL cohort overview. A total of 12 severe COVID-19 patients were included of which $n = 5$ were untreated controls and $n = 7$ received dexamethasone of which 3 deceased (for cohort details see Table S1).

(J) UMAP visualization of the cell types identified in the BAL of severe COVID-19 patients ($n = 67{,}439$ cells).

(K) Cell type marker for identification of present cell types identified in (H).

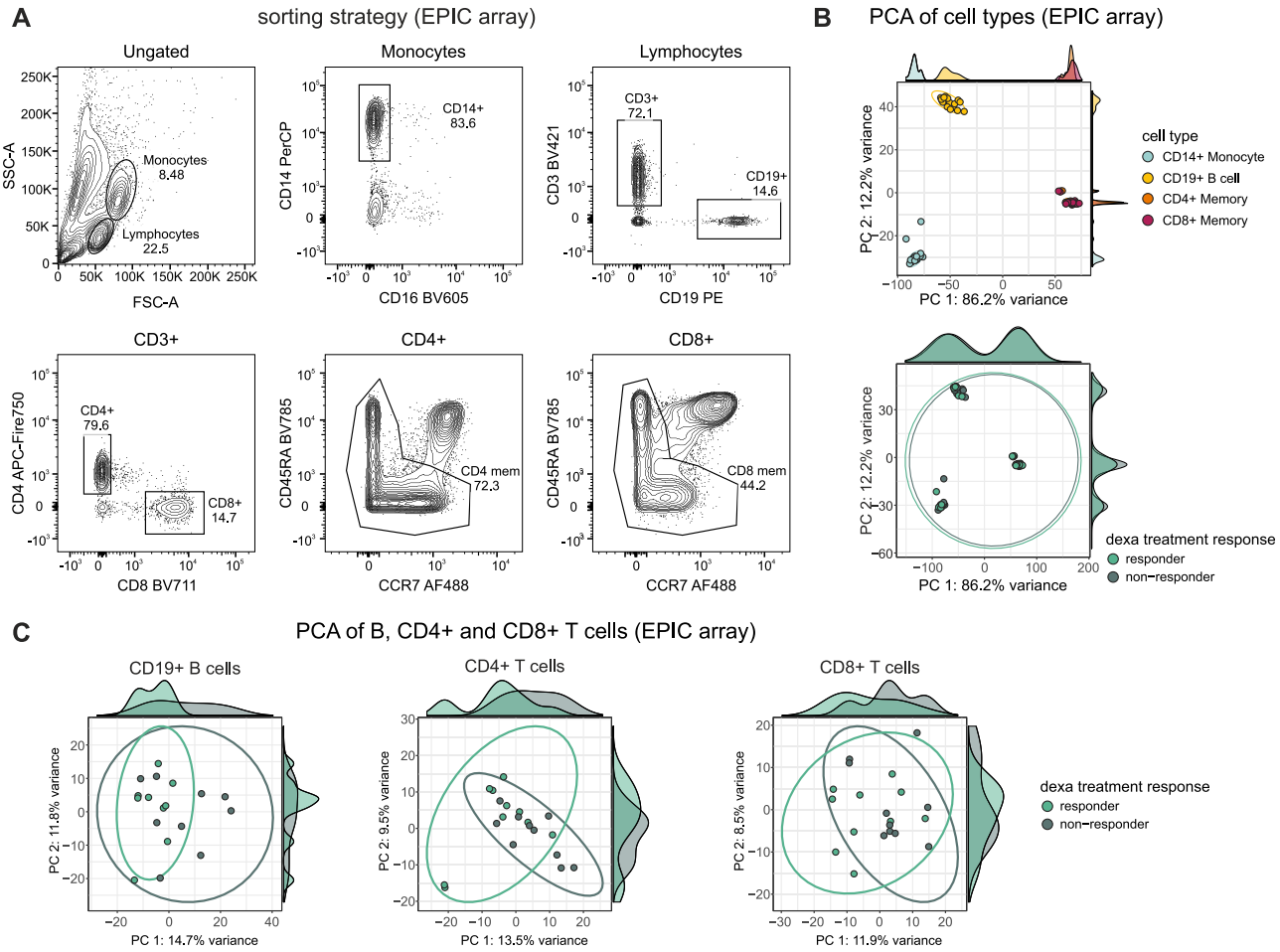

Figure S4. Gating strategy for cell sorting and PCA by treatment response of the epigenetic data, related to Figure 4

(A) FACS sorting strategy for the isolation of $CD14^{+}CD16^{-}$ monocytes, $CD19^{+}$ B cells, and $CD4^{+}$ or $CD8^{+}$ memory T cells for DNA methylation analysis.

(B) PCA of DNA methylomes of all samples analyzed, colored by cell types (upper) and dexamethasone treatment response group (lower).

(C) PCA of DNA methylomes of B cells, $CD4^{+}$ and $CD8^{+}$ memory T cells by dexamethasone treatment response.

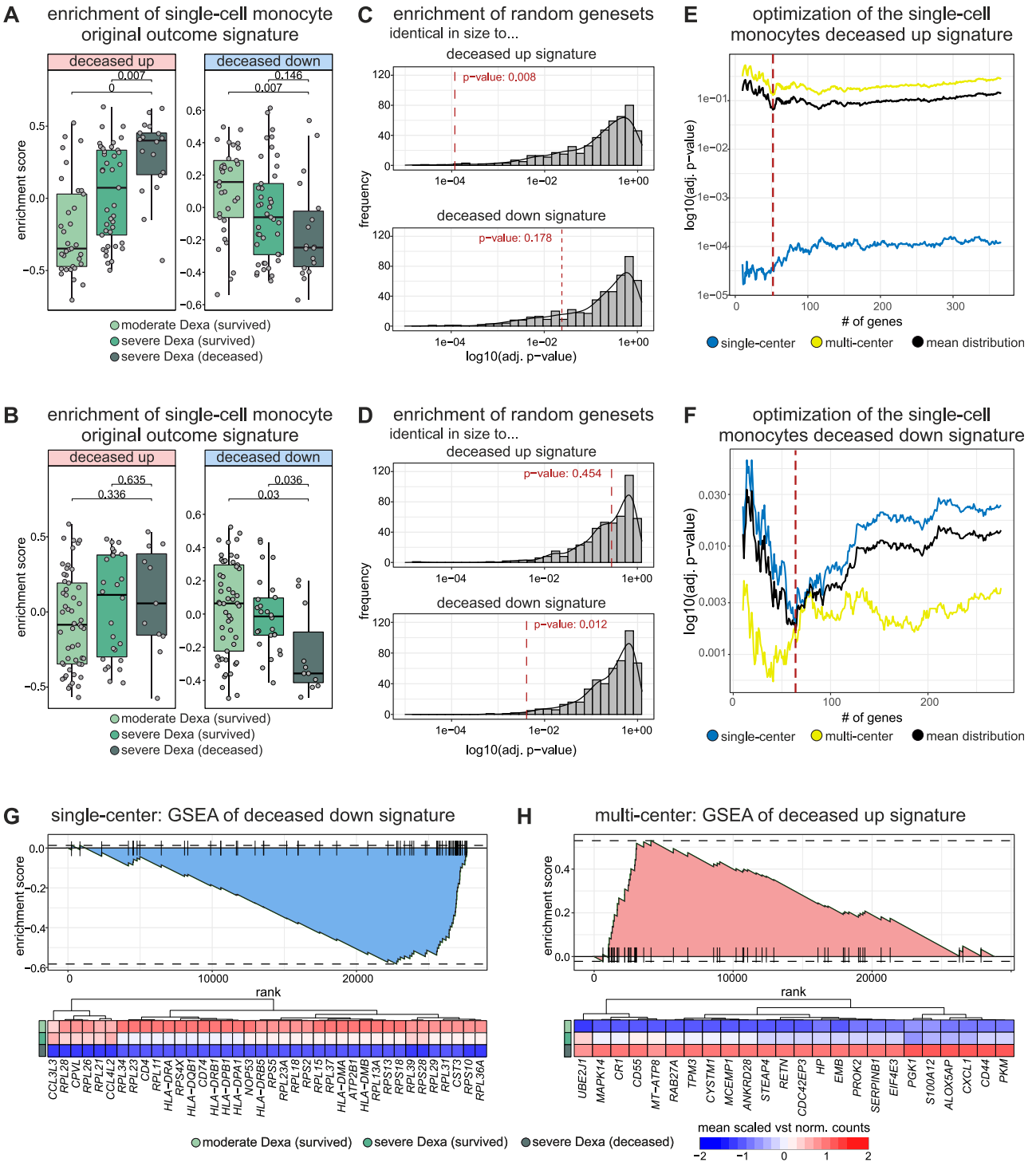

Figure S5. Optimization of the single-cell signature for enrichment in whole blood data, related to Figure 5

(A) Boxplots displaying the gene set variation analysis (GSVA) enrichment scores of the original deceased upregulated signature (left plot) and original deceased downregulated signature (right plot) in the single-center (Charité) cohort split and colored by the COVID-19 severity status and outcome. Wilcoxon test and Benjamini-Hochberg adjustment were utilized for statistical analysis.

(B) Boxplots displaying the GSVA enrichment scores of the original deceased upregulated signature (left plot) and original deceased downregulated signature (right plot) in the multi-center (CAPNETZ) cohort split and colored by the COVID-19 severity status and outcome. Wilcoxon test and Benjamini-Hochberg adjustment were utilized for statistical analysis.

(legend continued on next page)

(C) *p* value distribution of GSVA enrichment results of 500 random, unique gene sets in the single-center cohort on a $\log_{10}$ scale. Gene set size was based on the size of the original deceased upregulated signature (upper plot) and the original deceased downregulated signature (lower plot). *p* values were computed with a Wilcoxon test comparing deceased and surviving patients and were Benjamini-Hochberg adjusted. The red dashed line represents the adjusted *p* value from GSVA enrichment of the original deceased upregulated and the original deceased downregulated signatures, respectively.
(D) *p* value distribution of GSVA enrichment results of 500 random, unique gene sets in the multi-center cohort on a $\log_{10}$ scale. Gene set size was based on the size of the original deceased upregulated signature (upper plot) and the original deceased downregulated signature (lower plot). *p* values were computed with a Wilcoxon test comparing deceased and surviving patients and were Benjamini-Hochberg adjusted. The red dashed line represents the adjusted *p* value from GSVA enrichment of the original deceased upregulated and the original deceased downregulated signatures, respectively.
(E) Line plot of the deceased upregulated signature optimization illustrating the GSVA *p* value distribution between deceased and surviving patients with varying signature size based on the average $\log_2$FC from the scRNA-seq data. Signature size varied from 10 to the number of signature genes expressed in both cohorts, and the distributions were color-coded according to the single-center cohort (blue), the multi-center cohort (yellow), and the mean of the single- and multi-center cohorts (black). The red dashed line indicates the optimal gene signature size.
(F) Line plot of the deceased downregulated signature optimization illustrating the GSVA *p* value distribution between deceased and surviving patients with varying signature size based on the average log2FC from the scRNA-seq data. Signature size varied from 10 to the number of signature genes expressed in both cohorts, and the distributions were color-coded according to the single-center cohort (blue), the multi-center cohort (yellow), and the mean of the single- and multi-center cohorts (black). The red dashed line indicates the optimal gene signature size.
(G) Gene set enrichment analysis (GSEA) of the optimized deceased downregulated signature in the deceased patient group of the single-center cohort. Ranking of samples is based on expression-level statistics, and the running sum is visualized. The heatmap depicts the scaled variance-stabilized mean expression per COVID-19 severity status and outcome of the genes included in the leading edge.
(H) GSEA of the optimized deceased upregulated signature in the deceased patient group of the multi-center cohort. Ranking of samples is based on expression-level statistics, and the running sum is visualized. The heatmap depicts the scaled variance-stabilized mean expression per COVID-19 severity status and outcome of the genes included in the leading edge.